KTH Chemical Science
and Engineering

Adsorption of biopolymers and their layer-by-layer assemblies on hydrophilic surfaces

Maria Lundin

Doctoral Thesis

Stockholm, Sweden 2009

Akademisk avhandling som med tillstånd av Kungliga Tekniska Högskolan framlägges till offentlig granskning för avläggande av teknologie doktorsexamen fredagen den 9:e oktober 2009 klockan 13:00 i hörsal F3, Kungliga Tekniska Högskolan, Lindstedtsvägen 26, Stockholm.

Title: Adsorption of biopolymers and their layer-by-layer assemblies on hydrophilic surfaces

TRITA CHE-Report 2009:49
ISSN 1654-1081
ISBN 978-91-7415-419-1

KTH Royal Institute of Technology
School of Chemical Science and Engineering
Surface and Corrosion Science
Drottning Kristinas väg 51
SE-100 44 Stockholm

Printed at Universitetsservice US-AB

Abstract

It is widely known that surfaces play an important role in numerous biological processes and technological applications. Thus, being able to modify surface properties provides an opportunity to control many phenomena occurring at interfaces. One way of controlling surface properties is to adsorb a polymer film onto the surface, for example through layer-by-layer (LbL) deposition of polyelectrolytes. This simple but versatile technique enables various polymers, proteins, colloidal particles etc. to be incorporated into the film, resulting in a multifunctional coating. Due to recent legislations and a consumer demand for more environmentally friendly products, we have chosen to use natural polymers (biopolymers) from renewable resources.

The focus of this thesis has been on the adsorption of biopolymers and their layer-by-layer formation at solid-liquid interfaces; these processes have been studied by a wide range of techniques. The main method was the quartz crystal microbalance with dissipation monitoring (QCM-D), which measures the adsorbed mass, including trapped solvent and the viscoelastic properties of an adsorbed film. This technique was often complemented with an optical method, such as ellipsometry or dual polarization interferometry (DPI), which provided information about the “dry” polymer or protein adsorbed mass. From this combination, the solvent content and density of the layers was evaluated. In addition, the surface force apparatus (SFA), X-ray photoelectron spectroscopy (XPS), total internal reflection fluorescence (TIRF), and fluorescence resonance energy transfer (FRET) were utilized, providing further information about the film structure, chemical composition, and polymer inter-layer diffusion.

Adsorption studies of the glycoprotein mucin, which has a key role in the mucousal function, showed that despite the net negative charge of mucin, it adsorbed on negatively charged substrates. The adsorbed layer was highly hydrated and the segment density on the substrate was low. We showed the importance of characterizing the mucin used, since differences in purity, such as the presence of albumin, gave rise to different adsorption behaviours in terms of both adsorbed amount and structure. The adsorbed mucin layer was to a large extent desorbed upon exposure to the anionic surfactant sodium dodecyl sulfate (SDS). In order to prevent desorption, we demonstrated that a protective layer of the cationic polysaccharide chitosan could be adsorbed onto the mucin layer and that the mucin-chitosan complexes resisted the desorption normally induced by association with

SDS. Moreover, the association between chitosan and SDS was examined at the solid-liquid interface, in the bulk, and at the air-water interface. In all these environments chitosan-SDS complexes were formed and a net charge reversal of the complexes from positive to negative was observed when the concentration of SDS was increased.

Furthermore, the LbL deposition method could be used to form a multilayer-like film by alternate adsorption of mucin and chitosan on silica substrates. The LbL technique was also applied to two proteins, lysozyme and β-casein with the aim of building a multilayer film consisting entirely of proteins. These proteins formed complexes at the solid-liquid interface, resulting in a proteinaceous layer, but the build-up was highly irregular with an increase in adsorbed amount per protein deposition cycle that was far less than a monolayer.

Continuing with chitosan, known to have antibacterial properties we assembled multilayers with an anti-adhesive biopolymer, heparin, to evaluate the potential of this system as a coating for medical implants. Multilayers were assembled under various solution deposition conditions and the film structure and dynamics were studied in detail. The chitosan-heparin film was highly hydrated, in the range 60-80 wt-% depending on the deposition conditions. The adsorbed amount and thickness of the film increased exponential-like with the number of deposition steps, which was explained by inter-diffusion of chitosan molecules in the film during the build-up. In a novel approach, we used the distant dependent FRET technique to prove the inter-layer diffusion of fluorescent-labelled chitosan molecules within the film. The diffusion coefficient was insignificantly dependent on the deposition pH and ionic strength, and hence on the film structure. With the use of a pH sensitive dye buried under seven chitosan-heparin bilayers, we showed that the dye remained highly sensitive to the charge of the outermost layer. From complementary QCM-D data, we suggested that an increase in the energy dissipation does not necessarily indicate that the layer structure becomes less rigid.

Sammanfattning

Det är välkänt att ytor spelar en viktig roll i många biologiska processer och tekniska tillämpningar. Att kunna modifiera en ytas egenskaper ger därför en möjlighet att kunna kontrollera många fenomen som sker på ytor. Ett sätt att kontrollera ytegenskaperna är genom att adsorbera en polymerfilm på ytan, till exempel genom att växelvis adsorbera olika polyelektrolyter (LbL-teknik). Denna enkla men mångsidiga teknik möjliggör att många olika material kan införlivas i filmen, vilket resulterar i en multifunktionell beläggning. På grund av dagens lagstiftning och konsumenters ökade efterfrågan på miljövänliga material beslutade vi oss för att använda biologiska polymerer (biopolymerer) i detta projekt.

Fokus i den här avhandlingen har varit på adsorption av biopolymerer och deras LbL-formation på gränsytan vätska-fast fas, där adsorptionsförloppet och det adsorberade skiktet bestående av biopolymerer studerats med en mängd olika tekniker. Huvudtekniken var kvartskristallmikrovåg med energidissipations-registrering (QCM-D), som mäter massan inklusive inkorporerat vatten, samt de viskoelastiska egenskaperna hos ett adsorberat skikt. Som komplement till denna teknik användes ofta optiska metoder, till exempel ellipsometri och ”dubbel polarisationsinterferometri (DPI)”, två tekniker som endast mäter massan av de adsorberade biopolymererna. Genom denna kombination av metoder kunde massan av inkorporerat vatten i filmen och filmens densitet bestämmas. Dessutom användes ytkraftsapparaten (SFA), röntgenfotoelektronspektrometri (XPS), och fluorescens-spektroskopiteknikerna TIRF och FRET i några undersökningar för att erhålla information om skiktens struktur, kemiska sammansättning och polymerernas diffusion inom skiktet.

Adsorptionsstudier av glycoproteinet mucin, som har en central roll i funktionen av slemhinnan, avslöjade att trots att mucinet har en negativ nettoladdning adsorberade det ändå på negativt laddade substrat. Det adsorberade lagret var väldigt hydratiserat och hade en låg andel mucin i direkt kontakt med ytan. Vi påvisade vikten av att noga undersöka mucinet som användes, eftersom olika renhet, till exempel i form av förekomsten av albumin gav upphov till olika adsorptionsbeteende gällande både adsorberad mängd och struktur. En stor andel av det adsorberade mucinlagret desorberade när det exponerades för den anjoniska tensiden natriumdodecylsulfat, SDS. Vi visade att ett skyddande lager av den katjoniska polysackariden chitosan kunde adsorberas på mucinet och att mucin-chitosan-komplexen inte desorberade när SDS tillsattes.

Därtill studerades växelverkan mellan chitosan och SDS på gränsytan vätska-fast fas, i bulken och på luft-vattengränsytan. Komplex av chitosan-SDS bildades i samtliga miljöer och en nettoladdningsomsvängning från positiv till negativ observerades när koncentrationen av SDS ökades.

Vidare kunde LbL-tekniken nyttjas för att skapa ett multilagerlikt skikt genom att alternerande adsorbera mucin och chitosan på kiseldioxidsubstrat. Denna teknik användes även med två proteiner, lysozym och β-kasein, med målet att skapa ett multilager bestående av endast proteiner. Dessa proteiner bildade komplex på gränsytan vätska-fast fas i form av ett blandat proteinlager, men uppbyggnaden var väldigt oregelbunden med en ökning i adsorberad mängd per proteindeponeringscykel som var avsevärt mindre än ett monolager.

Inom området för biomaterial utgör de antibakteriella och antihäftande egenskaperna hos chitosan respektive heparin en lovande blandning för beläggningar av medicinska implantat. Baserat på detta konstruerade vi multilagerfilmer av chitosan och heparin med olika deponeringslösningar och undersökte dynamiken och filmens struktur i detalj. Chitosan-heparin-filmen var starkt hydratiserad, bestående av cirka 60-80 vikt-% vatten beroende på deponeringsbetingelserna. Den adsorberade mängden och tjockleken på filmen ökade nästan exponentiellt med antal deponeringar, vilket förklarades med chitosanets förmåga att diffundera genom filmen under uppbyggnaden. Med ett nytt angreppssätt använde vi FRET för att bevisa diffusionen av fluorescerande färgmärkt chitosan i filmen under uppbyggnaden. Diffusionskoefficienten var i princip oberoende av pH och jonstyrka under deponeringen och följaktligen av filmens struktur. Genom att använda ett pH-känsligt färgämne begravt under sju biskikt av chitosan-heparin visade vi att färgämnet i hög grad påverkades av laddningen på det yttersta lagret. Från QCM-D-data lade vi fram teorin om att en ökning av energidissipationen för ett lager inte nödvändigtvis indikerar att lagrets struktur har blivit mindre styvt.

List of papers included in the thesis

I. **A Comparison of the Adsorption Kinetics and Surface Arrangement of "As Received" and Purified Bovine Submaxillary Gland Mucin (BSM) on Hydrophilic Surfaces**
Lundin, M.; Sandberg, T.; Caldwell, K.D.; Blomberg, E.
Journal of Colloid And Interface Science, ***2009***, *336, 30-39*

II. **Mucin-chitosan complexes at the solid-liquid interface: Multilayer formation and stability in surfactant solutions**
Dedinaite, A.; Lundin, M.; Macakova. L.; Auletta, T.
Langmuir, ***2005***, *21, 9502-9509*

III. **Interactions between chitosan and SDS at low charged silica substrate compared to interactions in the bulk. The effect of ionic strength**
Lundin, M.; Macakova, L.; Dedinaite, A.; Claesson, P.
Langmuir, ***2008***, *24, 3814-3827*

IV. **Adsorption of lysozyme, β-casein and their layer-by-layer formation on hydrophilic surfaces: effect of ionic strength**
Lundin, M.; Elofsson, U. M.; Blomberg. E.; Rutland, M. W.
Submitted to Colloids and Surfaces B: Biointerfaces

V. **Layer-by-layer assemblies of chitosan and heparin: effect of ionic strength and pH**
Lundin, M.; Solaga, F.; Thormann, E.; Blomberg, E.
Manuscript

VI. **Polymer dynamics in layer-by-layer assemblies of chitosan and heparin**
Lundin, M.; Blomberg, E.; Tilton, R. D.
Submitted to Langmuir

Contribution by the respondent

I. Main author of the paper and did major part of the experimental work. ELLA/ELISA/mBCA measurements and protein purification were carried out by T. Sandberg.

II. Was involved in performing and analyzing ellipsometry measurements, and a minor part in the writing.

III. Prepared the paper together with M. Macakova. Was involved in all experimental work except performing ellipsometry measurements.

IV. Main author of the paper and performed all experimental work.

V. Main author of the paper and performed all experimental work, except for the contact angle measurements.

VI. Main author of the paper and did all experimental work. However, calculations of the diffusion coefficients, were carried out by R.D. Tilton.

Other papers not included in the thesis

VII. Soluble Complexes in Aqueous Mixture of Low Charge Density Comb Polyelectrolytes and Oppositely Charged Surfactants Probed by Scattering and NMR
Bastardo, L. A.; Iruthayaraj, J.; Lundin. M.; Dedinaite, A.; Vareikis, A.; Makuska, R.; van der Wal, A.; Furo, I.; Garamus, V. M.; Claesson, P. M.
*Journal of Colloid And Interface Science**, 2007**, 312, 21-33*

VIII. Adsorption of IgG on/in a PAH/PSS multilayer film; layer structure and cell response
Feldötö, Z. Lundin, M.; Blomberg, E.
Manuscript

Table of Contents

1 Summary of Papers

Paper I

The large glycoprotein, mucin, is the major protein constituent in for example saliva and on mucosal membranes. The bovine submaxillary mucin (BSM) has often been used to mimic mucosal membranes and in surface coatings to prevent bacterial adhesion on solid biosurfaces. However, the as received commercial grade BSM has been found to contain significant amounts of non-mucin material, where albumin (BSA) was identified as the dominant protein contaminant. Due to this finding, our aim was to investigate how the presence of BSA in a BSM solution affects the adsorption of BSM to negatively charged hydrophilic surfaces. The results showed that the level of BSM purification had a large impact on the adsorbed layer in terms of amount and layer structure. With the SFA technique it was shown that the adsorption of further purified BSM (free from BSA) resulted in a much thinner adsorbed layer compared to that adsorbed from as received BSM. The difference was suggested to be due to the presence of BSA in the layer adsorbed from as received BSM. The BSA content in the as received starting material was estimated to be up to 9 wt-%. However, it was found that the layers formed on mica after adsorption from a pre-equilibrated BSM:BSA mixture having a BSA content in the range 5-9 wt% gave a higher BSA content in the layer compared to the layer adsorbed from as received BSM. Further, adsorption from pre-equilibrated mixtures of BSM and BSA showed that an increased fraction of BSA to BSM in solution resulted in formation of a dense and rigid layer in comparison to the highly expanded layer of BSM. Furthermore, BSA was the predominant species in the BSM-BSA mixed layers adsorbed from an equal amount of BSM and BSA (50 wt-% BSA).

Paper II

In this paper we investigated the stability of a mucin layer adsorbed from as received BSM on negatively charged surfaces, towards exposure of the anionic surfactant sodium dodecyl sulfate (SDS). This surfactant is a commonly used detergent in personal care products e.g. toothpaste, and the BSM layer can be viewed as a simplified model of the oral cavity. The results showed that BSM associates with SDS already at low surfactant concentrations and

that approximately 80 % of the initially adsorbed amount is desorbed upon addition of SDS at a concentration equal to its critical micellar concentration. In order to prevent BSM desorption by SDS, a protective layer of the naturally occurring cationic polysaccharide chitosan was adsorbed onto the preadsorbed BSM layer on silica or mica prior to addition of SDS. It was shown that chitosan adsorbed on BSM and that the BSM-chitosan complexes were resistant towards desorption induced by SDS. Further, we showed that BSM and chitosan could be used to form a multilayer film by sequential adsorption of BSM and chitosan on a silica substrate.

***Paper* III**

The interaction between chitosan and SDS, observed in paper II, was further investigated in this paper. Two different systems were investigated and compared: the association between SDS and preadsorbed chitosan on a silica substrate, and the chitosan-SDS association in bulk solution. Both systems were followed as a function of solution ionic strength and surfactant concentration at pH 4. It was shown that chitosan and SDS formed complexes in solution that were far more surface active than the surfactant alone. Both in solution and at the solid-liquid interface, the number of SDS to chitosan could exceed one, which resulted in a charge reversal from positive to negative of complexes at higher surfactant concentrations. At the solid–liquid interface, the association was highly dependent on the chitosan layer structure on silica. A flat rigid layer of chitosan was formed at 0.1 mM $NaNO_3$, whereas more extended layers were formed from solution of 30-500 mM $NaNO_3$ and no adsorption was observed from a 1000 mM $NaNO_3$ solution. In 30 mM $NaNO_3$ and upon increasing the amount of SDS the chitosan layer went through a compaction at low surfactant concentrations followed by reswelling and finally layer desorption. No layer compaction could be observed upon addition of SDS to the thin chitosan layer adsorbed from 0.1 mM $NaNO_3$. Instead, there was a continuous increase in layer viscoelasticity before desorption occurred.

Paper IV

In paper II we showed that a multilayer film could be formed by sequential adsorption of a protein (BSM) and the polysaccharide chitosan. The aim of this project was to investigate the possibility of forming a multilayer film containing only proteins, namely

lysozyme and β-casein. These proteins were sequentially adsorbed on silica from a solution of pH 8.5, which ensured that lysozyme was net positively charged and β-casein net negatively charged. Particular emphasise was placed on finding a suitable ionic strength of the deposition solution at which the two oppositely net-charged proteins could form a multilayer-like film. This was observed at intermediate and high ionic strength in comparison to low ionic strength. However, independent of solution conditions the growth in adsorbed amount was highly irregular during the build-up, and the adsorbed amount of protein after each deposition was far less than a monolayer. Even so, the amount of lysozyme and β-casein in mixed layers exceeded that of pure lysozyme or β-casein layers on silica. Clearly, the film contained both proteins but the film structure was different from that usually observed for multilayer films using polyelectrolytes. The reason for the observed difficulty in forming a pure protein film was probably due to the complex charge distribution and structure of proteins in comparison to polyelectrolytes.

Paper V

Multilayer films of chitosan and heparin were formed on silica surfaces with the LbL deposition method. A combination of these two polysaccharides has previously been shown to suppress bacterial adhesion on surfaces, where the efficiency was largely dependent on the solution deposition pH, hence on the formed layer structure. Several different techniques were therefore used to study the structure of the chitosan-heparin complexes adsorbed at the solid-liquid interface depending on the solution deposition conditions (e.g. pH and ionic strength). All films were, independent of deposition conditions, highly hydrated and even after the formation of six chitosan-heparin bilayers the relative solvent content was very high (60-80 wt-%). The general trend was that the adsorbed layer became increasingly dense with the number of deposited layers. The film structure was highly dependent on both the solution conditions and on the polymer adsorbed in the outermost layer. For the deposition conditions favouring a strong binding between oppositely charged polysaccharides, the film structure (viscoelesticity) could not be accurately determined from the measured layer energy dissipation. Instead we showed using a Voight based model that a measured increase in energy dissipation from an adsorbed layer could be observed even when a layer changes its overall structure from less to more rigid. Another

interesting finding was that the layer thickness (and adsorbed amount) increased exponential-like with the number of deposited layers. This phenomena has been observed previously for some other multilayer films consisting of polysaccharides and/or polypeptides and has been ascribed to interlayer diffusion of at least one of the two polyelectrolytes within the film during build-up. This finding initiated the work carried out in paper VI.

Paper VI

The aims of this paper were to investigate whether the exponential-like growth in thickness of chitosan and heparin multilayers was due to interlayer diffusion of chitosan molecules and if the diffusion depended on the film structure, hence on the solution deposition conditions. For this purpose chitosan molecules were labelled with a fluorescence dye and the distant dependent fluorescence resonance energy transfer (FRET) technique was used. To our knowledge this is the first work in which FRET has been used to study interlayer diffusion of polysaccharides. The advantage of FRET is the possibility to monitor polymer diffusion in much thinner films compared with the commonly used confocal laser scanning microscopy (CLSM) technique. The results confirmed that chitosan diffuses in the film during deposition and that the diffusion coefficient is largely independent of the deposition conditions used in this work. The internal structure of the chitosan and heparin layers was further evaluated by the use of a fluorescence dye, which is sensitive to the electrostatic potential in its environment. These results were compared to previously reported data using strong synthetic polyelectrolytes. From this comparison it was found that the chitosan-heparin multilayer film is highly interpenetrated in comparison to multilayers consisting of synthetic polyelectrolytes.

2 Introduction

In this work, several independent but related projects were carried out with the aim of improving the understanding of biopolymer adsorption and their layer-by-layer deposition at the solid-liquid interface. The biopolymers focused on in these studies were natural polysaccharides (chitosan and heparin) and proteins (mucin, lysozyme, and β-casein), that all come from renewable resources. The large attractiveness in working with these materials is that, in comparison to most synthetic polymers, they are biocompatible, biodegradable, and show a low-toxicity. For these reasons, they are already widely used in the pharmaceutical and food industry.

Our interest has been to gain a fundamental understanding of the adsorption process occurring in each of the investigated model systems. However, these systems are not only of academic interest as will be described below before entering into a more detailed description of our aims. Our adsorption studies were carried out on solid planar supports and therefore the most relevant application is for biopolymer coatings for medical implants. The surface properties of a material can be altered by adsorption of polymers and/or proteins, which thereby alter the affinity for bacterial and cell adhesion. One example is the mucin proteins that when adsorbed on polymeric surfaces have been found to reduce bacterial and cell adhesion.[1,2,3] Further, multilayer complexes of chitosan and heparin adsorbed on PET surfaces have proven highly efficient in not only reducing bacterial adhesion, but also in killing bacteria that did adhere.[4] Both the mucin and the chitosan-heparin layer coatings are highly hydrated by water, which has been the suggested reason for the efficiency of other polysaccharide based coatings in inhibiting cell attachments.[5,6,7] The improved functionality of a coating containing more than one component, such as the chitosan-heparin multilayer film, has also been used with embedded proteins within polymer coatings. Direct contact with a solid surface often affects the structure and hence the biological activity of a protein such as e.g. lysozyme, whereas the protein maintains its biological activity to a higher extent within the layer.[8, 9]

This work can be divided into three major parts:

1. The adsorption and structure of mucin on negatively charged surfaces was studied based on the level of purification, essentially on the level of protein (albumin) present in solution. Further, we elucidated the possibility of using a protective layer of the cationic polysaccharide (chitosan) adsorbed onto the pre-adsorbed mucin layer to hinder desorption induced by the anionic surfactant SDS. The main methods used to characterize the adsorption of mucin and its interactions with albumin, chitosan, and SDS, were the surface force apparatus (SFA), X-ray photoelectron spectroscopy (XPS) and ellipsometry that together provide information on the thickness, structure and chemical composition of an adsorbed layer.

2. In a smaller part of the thesis we investigated and compared the interactions between oppositely charged chitosan and SDS at the solid-liquid interface and in bulk solution, and further how these interactions depended on the solution ionic strength. This is discussed in paper III, but only the interactions at the solid-liquid interface are presented in the summary of key results (chapter 4), since the thesis deals with interactions at the solid-liquid interface.

3. The last part, which is the major part of the thesis, deals exclusively with the concept of multilayer films formed with the layer-by-layer (LbL) method. Experiments were carried out by alternate adsorption of oppositely charged polymers (polysaccharides or proteins) on negatively charged hydrophilic substrates. First, we investigated the possibility of forming a multilayer film using a large flexible glycoprotein (mucin) and a polysaccharide (chitosan). Next, we explored if it was possible to adjust the solution deposition conditions in such a way that multilayer-like films consisting of only proteins (lysozyme and β-casein) could form. Finally, inspired by the promising results for chitosan-heparin films as anti-bacterial and anti-adhesive coatings on medical implants,[4] we built multilayers with two polysaccharides (chitosan and heparin) and investigated their build-up and structure under various deposition solution conditions in great detail. A combination of seven different surface sensitive techniques was employed in order to obtain a broad view of the adsorbed layer structure, and on the kinetics of adsorption.

2.1 Background

2.1.1 Polyelectrolytes and proteins

Polyelectrolytes are polymers, in which all or some of the monomers are electrically charged. One can distinguish between two kinds of charged monomers (which are related to their chemical composition). Monomers that contain permanent charges e.g. the quaternary ammonium group, and monomers containing ionisable groups, e.g. primary amines and carboxylic acids that can dissociate in solution depending on the pH and ionic strength. The charge is then related to the degree of ionisation in solution. The pH at which 50 % of the ionisable monomer groups are charged is given by the pKa of the ionisable group. Polyelectrolytes are often referred to as weak or strong depending on the pKa value of their monomer groups. Strong polyelectrolytes are fully charged over a broad range of pH values (~2-10), whereas weak polyelectrolytes are partially charged in this range. The polymer charge density largely affects the conformation, which can be altered by adjusting the solution ionic strength (screening of electrostatic repulsive forces) and for weak polyelectrolytes also by the pH. Further, there are several types of polyelectrolytes but a distinction can be made between synthetic polymers and the natural polysaccharides (sugar based) and polypeptides (amino acids). In this work, we have focused on two natural polysaccharides, one strong (heparin) and one weak (chitosan).

Proteins are a large group of natural polymers (polypeptides) formed by a number of amino acids. They are generally more complex, both in composition and structure, compared to polyelectrolytes due to the many different amino acids in their repeat unit that makes them into polyampholytes. Since every amino acid has a different pKa value, it is common to refer to their net charge as negative (above iep) or positive (below iep), where the isoelectric point (iep) defines the solution pH where the net charge is zero. Based on their three-dimensional structure, proteins may be classified into three different categories, globular, flexible, and fibrous.[10] In this work, proteins belonging to the two first classes have been studied.

2.1.2 Adsorption of macromolecules at solid surfaces

Adsorption at an interface such as the solid-liquid interface occurs due to a decrease in the total free energy of the system. There are several contributions to the overall adsorption process: electrostatic forces, entropy, hydrophobic interactions, hydrogen bonds, and van der Waals forces. The significance of these interactions in a given system depends on the polymer

structure/composition, solvent, and on the surface involved. The adsorption process is generally determined by the Gibbs free energy of adsorption (*G*), which depends on enthalpy (*H*), entropy (*S*), and temperature (*T*). Adsorption occurs at the interface if the change in Gibbs free energy (ΔG_{ads}) due to the adsorption process is negative.

$$\Delta G_{ads} = \Delta H_{ads} - T\Delta S_{ads} \qquad (2.1)$$

Enthalpic driving forces include attractive van der Waals interactions and attractive or repulsive electrostatic interactions between the polymer and the interface, and between polymer molecules. Entropic contributions may arise from: changes of the polymer conformation upon adsorption, liberation of counter-ions from a charged surface and the polymer, and from hydrophobic interactions such as surface dehydration. These interactions have been thoroughly described for protein adsorption by Norde and co-workers[11,12] and for polymer adsorption by Fleer and co-workers.[13]

It is difficult to make a general statement regarding the driving force of polymer adsorption, since polymers constitute such a diverse family ranging from highly flexible polymers to compact and structured proteins (globular protein), as discussed in section (2.2.1). In spite of showing many common features, the adsorption of polymers of these two extreme cases, is different in several ways. For example, the adsorption of a globular protein results in a small conformational change without the formation of loops and tails as is commonly discussed for flexible polymers.[13] Further, the entropy change resulting from the conformational change upon adsorption often favours the adsorption of globular proteins, whereas it restricts adsorption of flexible polymers.[12] Even though globular proteins exhibit small structural changes, they are very often an important, if not the most important, driving force for adsorption. This is true for adsorption on hydrophobic surfaces and also on hydrophilic surfaces when the protein has a relatively low conformational stability (e.g. albumin), but not when the conformational stability is high (e.g. lysozyme). In the latter case, adsorption occurs only if the substrate and protein are oppositely charged, due to electrostatics and to liberation of counter-ions resulting in an increase in entropy. For a flexible charged polymer (polyelectrolyte), the loss in conformational entropy will in most cases be compensated for by the gain in translation entropy, which is caused by the release of small ions. Moreover, the structure of the adsorbed polyelectrolyte, hence its extension into the solution (fraction between trains, loops, and tails) depends on the charge density of the substrate, the polyelectrolyte, as well as on the solution conditions.[13]

2.1.3 Biomaterial coatings using mucin proteins

In the field of biomaterials it has become increasingly popular to construct material coatings based on natural polymers to control the surface properties of man-made materials. Mucins are a family of natural glycoproteins with important functions in the mucous gel, which covers the ephitelial cell surfaces. The function of mucins is to act as a steric barrier and prevent non-specific interactions of proteins and cells with the underlying cell membrane and further to keep mucous lubricated and hydrated.[2,14] In order to mimic nature, polymeric biomaterial surfaces have been coated with mucins, resulting in the reduction of bacterial and cell adhesion.[1,2,3] Adsorbed layers of mucins on solid surfaces have also been used to model mucous for e.g. oral drug delivery studies[15], dental applications[16,9], and to test its stability towards oral care products (surfactants).[9,17] A detailed fundamental understanding of the adsorption of mucins, isolated from different regions and species, on solid surfaces has been carried out in the past. Several of these studies have involved the bovine submaxillary gland mucin (BSM) due to its early commercial availability and its extensive usage.[18,19,16,17] These studies have shown that BSM generally has a higher affinity for non-polar surfaces compared to polar-charged surfaces, and least affinity for polar uncharged surfaces.[20,16] Further, on polar-negatively charged surfaces adsorption is favoured when the solution ionic strength is increased, due to a decreased electrostatic repulsion between the net negative BSM molecules (iep=3)[18] and the substrate at pHs above 3.[16]

2.1.4 Layer-by-layer (LbL) self-assemblies

Various methods have been used to prepare thin films on solid surfaces, such as Langmuir-Blodgett (LB), self-assembled monolayer (SAM) and layer-by-layer (LbL) self-assembly. An advantage with the LBL method is that multilayered films can be formed on essentially any type of charged substrate regardless of size and shape, by alternating adsorption of oppositely charged compounds. The method was initiated in the pioneer work by Iler in the field of colloidal particles (1966).[21] However, the large interest in the technique began in the early 1990s, when Decher et *al.* showed that this method could be applied also to polyelectrolytes.[22] Ever since, there has been a tremendous interest in the technique with several hundred publications every year where the LbL method has been employed. Figure 2.1 shows a schematic of the LbL adsorption method using polyelectrolytes. A substrate with a charged surface is immersed in a solution of oppositely charged polyions, (1). The adsorption of polyions on the surface often results in an overcompensation of the substrate charge which consequently reverses the sign of the surface charge. After rinsing (2)

in a pure electrolyte solution the assembly is immersed in a solution of oppositely charged polyions, (3), resulting in further adsorption and a new reversal of the surface charge followed by rinsing (4). The procedure is then continued until the desired layer thickness is obtained.

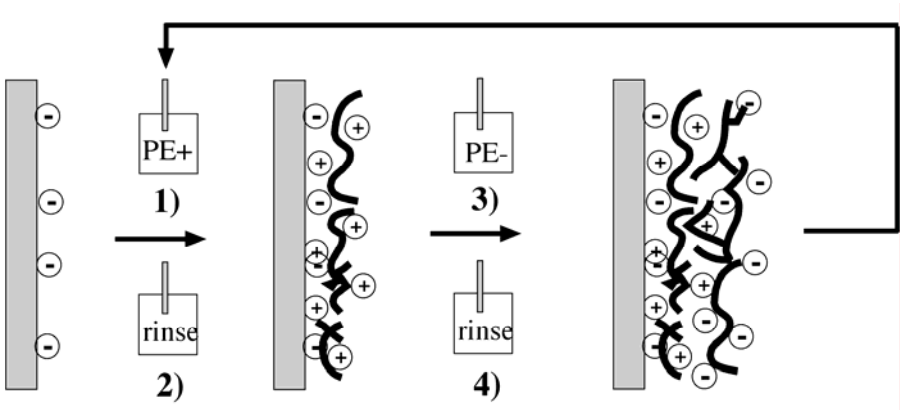

Figure 2.1. *The multilayer build-up using the LbL method.*

The charge overcompensation by adsorbing polyelectrolytes leading to the reversal of surface charge is considered to be a requisite for multilayer formation, since it enables subsequent adsorption of oppositely charged polyelectrolytes to the next layer.[23, 24] The charge inversion has been experimentally verified for many polyelectrolyte pairs.[25,26,27] However, the mechanism behind recharging and the driving forces for the build-up are still not fully understood. In early publications, it was suggested that the electrostatic interactions between opposite charges was the driving force for the build-up. The finding that a minimum charge density of a polyelectrolyte is needed for successful layer growth further supported that theory.[28] However, from an electrostatic point of view, the adsorption is likely to stop when the polyelectrolyte-coated substrate has a zero surface charge. Further, multilayers can be formed in solution at high ionic strength, where the electrostatic attraction will be screened.[29] Other non-electrostatic interactions, such as hydrogen bonding, hydrophobic interactions, and entropy must therefore play an important role in the multilayer formation as suggested in a number of studies.[30,31,32,29] The multilayer build-up is then a result of both electrostatic and non-electrostatic interactions. In fact, the main driving force for the build-up has later been attributed to the gain in entropy due to liberation of counterions and water of hydration upon adsorption.[29,33]

One major advantage with the LbL deposition technique is that it permits construction of films containing other macromolecules, such as proteins, enzymes, or nucleic acids.[34] In the past, mixed layers of different polyelectrolytes and water soluble proteins have been successfully formed[35,36,37], where the secondary structure of the protein has been found to be close to that of their native form in solution.[8] Embedded proteins in multilayers are therefore prone to maintain their enzymatic activity compared to those in direct contact with a solid substrate.[9]

2.1.5 Layer structure and film growth of LbL films

The multilayer-film structure and thickness can be controlled by changes in the solution deposition conditions, e.g. by solution ionic strength and for weak polyelectrolytes also by pH. Generally, an intermediate polyelectrolyte charge density and/or a high solution ionic strength results in significantly thicker films compared to highly charged polymers adsorbed from low ionic strength solutions.[24,38,29] This is due to a decreased repulsion between charges along the polymer chain resulting in a coiled-like polymer structure and hence a larger thickness and adsorbed amount. However, there is an upper limit for the ionic strength, above which complexes are not formed.[39]

The film structure is further dependent on the polyelectrolyte pair used. For example, there have been mainly two types of film growth reported in the literature, namely: film thickness and adsorbed amount increase either linearly or exponentially with the number of deposited layers. This topic has been thoroughly described in recent reviews by von Klitzing[29] and Picart[7]. The linear growth is common for strong synthetic polyelectrolytes, whereas an exponential-like growth can be found for some weak natural polyelectrolytes, typically polypeptides or polysaccharides.[40,5,29] One explanation to the observed exponential growth is provided by the diffusion theory, where at least one of the two polyelectrolytes diffuses within the film.[40] The theory states that the adsorbed amount in a given deposition step not only depends on the amount of oppositely charged polymer in the outermost layer, but also on the amount of free, diffusing polyelectrolytes available for complexation within the film. The amount of free polyelectrolytes is then proportional to the multilayer thickness (volume) prior to deposition. The confocal laser scanning microscopy (CLSM) technique has been used to visualize the out-of-plane (vertical) diffusion of fluorescence labelled polyions within very thick (several μm) films during build-up.[6,41,42] It has been suggested that a linear growth can be turned into an exponential growth if the LbL conditions are changed such that the

intermolecular interactions between the polyelectrolytes are sufficiently weakened.[43]

2.1.6 Potential applications for LbL films

A wide range of potential applications has been suggested for the multilayer films in such diverse areas as drug delivery systems[44], micropatterning[45], biomedical applications[46], food applications[47], and paper making. A few of these will be discussed here. The multilayer-film coatings can be prepared on both planar substrates and on colloidal particles. From the latter, hollow capsules can be prepared by dissolution of the particle core after the multilayer-film preparation.[44] The hollow capsules can then be loaded with pharmaceuticals and by choosing the right polymer pair, for the coating, it is possible to control the release rate from these capsules. On planar substrates there have been much research on antibacterial coatings for surfaces in contact with body fluids both in-situ and ex-situ.[4,46,48] The selection of suitable polymers together with the possibility of incorporating any type of charged molecule into the film enables the formation of surfaces that are cell/protein attractive or repellent.[46] In packing applications for example of food, both oxygen and water barriers are required in order to prevent oxidation of food products during transportation. A commercial product on the market is the fruit bags (Yasa-sheet) that keep vegetables and fruits fresh for weeks by reducing the emission of ethylene gas. These fruit bags are prepared from LbL deposition of chitosan and an enzyme extracted from bamboo (Figure 2.2).

Figure 2.2. *The result of using the Yasa-sheets invented by S. Shiratori, Japan, to extend the freshness of fruits. The figure was adapted from the homepage: (http://www.nasuden.co.jp/yasa.htm).*

Another interesting development on the market is the so-called “Metal Rubber” from NanoSonic Inc. This material, which is prepared by the LbL method using charged carbon particles on solid substrates show remarkable properties. As the name suggests, “Metal Rubber” combines the properties of rubber and metal, resulting in a material that can be heated, frozen, and exposed to jet fuel, and still retain its electricity-conducting properties. Future uses of the material may include artificial muscles, electrically charged aircraft wings, and protective clothing.

3 Experimental

Brief accounts of the most important methods and materials used in this work are given below, with the main emphasis on the most important characteristics for the experiments conducted. For a more detailed description the reader is referred to the appended papers.

3.1 Overview of experimental techniques

The main information that can be obtained from the experimental techniques used in this work is provided together with relevant references in Table 1 and 2. A few of the techniques are discussed further in section 3.2-3.6.

Table 3.1. *An overview of the surface analytical techniques used in this work to characterize the adsorbed layers.*

Adsorbed layers on solid surfaces	
Technique	**Information**
QCM-D[49,50,51]	Total mass including coupled solvent and information on the layer viscoelasticity measured *in-situ*
Ellipsometry[52,53,54]	Thickness, refractive index, and adsorbed amount of an adsorbed layer measured *in-situ*
DPI[55,56]	Thickness, refractive index, and adsorbed amount of an adsorbed layer measured *in-situ*
TIRF[57,58]	Amount of adsorbed fluorescent molecules measured *in-situ*
FRET[59,60]	Distance between two different fluorescent molecules measured *in-situ*
SFA[61,62]	Surface forces, layer thickness (extended and compressed), and layer compressibility
XPS[63,64]	Chemical composition of an adsorbed layer
AFM-imaging[65]	Surface topography

All the techniques listed in Table 3.1 have important advantages, but also some limitations. However, by using a combination of several techniques, many of these limitations can be overcome, and a broader view can be obtained. What follows below is a summary of essential advantages and limitations of the techniques used in this thesis, and a discussion regarding the benefits obtained when combining these methods.

In QCM-D, a large number of surface coatings on the quartz substrate can be used and measurements can be carried out in turbid solutions. However, it is difficult to decouple changes in mass from structural changes. The sensed mass includes trapped solvent, which can be used as an advantage when combined with another technique measuring the “dry” mass, and thereby the water content can be estimated.

Several optical methods, such as ellipsometry and DPI can be employed to determine the “dry” mass. In ellipsometry, the substrate needs to be smooth and reflective, and the ambient media have to be transparent. A large difference in refractive index between substrate, adsorbed layer, and ambient is preferable. The ellipsometry technique has the advantage that it also can measure relatively thick adsorbed films > ~ 200 nm, whereas QCM-D, DPI, and TIRF are restricted to the distance set by the penetration dept of an evanescent wave or an oscillating wave into the bulk solution. The DPI technique can be used in turbid solutions and is more accurate in the determination of both thickness and refractive index compared to ellipsometry. However, one major disadvantage of DPI is the limitation in substrate, since a waveguide (silica doped with nitrogen) has to be used.

An advantage with TIRF is the possibility of separating two different species in a film by fluorescence labelling. Though, the use of fluorescence techniques is always uncertain due to the fact that the dye may alter the polymer structure and affinity for a substrate. Further, changes in emission intensity may be caused by electrostatic potential changes in the environment.

With SFA the absolute thickness, and not an average thickness for a homogenous film as for DPI and ellipsometry is measured, but the limitation is the need for very smooth transparent substrates.

XPS has the limitation that adsorbed layers in solution can not be measured, since it requires ultra high vacuum. AFM suffers from the problem that a good resolution of the images is difficult to obtain with soft surfaces.

Table 3.2. *The techniques used to characterize interactions in the bulk*

Interactions in the bulk solution	
Technique	**Information**
Tensiometry[66]	Surface tension, critical micellar concentration (cmc)
Elecrophoretic mobilility[67]	Sign (positive or negative) of a charged polymer and polymer-surfactant complex
Turbidimetry	Qualitative information on the aggregation of complexes

3.2 Quartz crystal microbalance with dissipation (QCM-D)

A QCM-D instrument is basically a highly sensitive balance, which measures the amount of material added to or removed from an oscillating piezoelectrical quartz surface. The change in mass, *m*, of the surface due to adsorption will be observed as a change in the resonance frequency, *f*, where an increase in mass is observed as a decrease in the resonance frequency. Unlike most optical techniques the sensed mass includes mechanically trapped or bound solvent. The instrument also provides information on the viscoelastic properties (rigidity) of the adsorbed film since the energy dissipation, *D*, from the system is measured as the rate of decay of the oscillating amplitude when the voltage (driving the oscillation) is turned off. The theory of the technique has been thoroughly described by Rodahl et *al*.[49]

Two different instruments were employed in this study, a D300 (paper I, III, IV) and an E4 (paper V) system from Q-sense AB. The systems provide essentially the same information but the E4 unit is superior in that it has four independent measurement chambers that can run simultaneously, whereas the D300 has only one. Further, the E4 measures changes in frequency, *f*, and dissipation, *D*, at six different overtones instead of three (D300). The overtone number, *n*, indicates the frequency at which the quartz substrate oscillates, where 5 MHz is the fundamental tone (n=1) and the first overtone is n=3 (15 MHz) and so on. The different overtones penetrate the liquid to different depths. In each case the sensitivity decays exponentially. The decay-length for some of the overtones are: 240 nm (n=1), 140 nm (n=3), and 65 nm for n=13 in water at T=25° C.[50] However, the main reason for using the E4 unit in paper V was that it has a flow system incorporated with the same design as other techniques that were used. This means that the results are more comparable, since the flow of molecules over the surface is similar.

Several different models have in the past been suggested to relate the measured frequency change, *f*, into mass, *m*. In this work, three different models have been utilized, the Sauerbrey equation[68], Johannsmann model[69] and Voight model[50]. These models and the results obtained with them have been compared in a recent investigation by Iruthayaraj et al.[51] In that study the sensed mass calculated using the Sauerbrey and the simplified Johannsmann equation was fairly similar, whereas both models estimated a sensed mass considerably lower in comparison to the Voight model (for viscoelastic films). For example, in paper V, we showed that the estimation of sensed mass using Sauerbrey could be as low as 60 % of the Voight value for films showing high-energy dissipation values.

The Sauerbrey equation[68] is the simplest and most commonly used equation, which states a linear relation between the measured frequency change due to adsorption compared to the plain quartz crystal, Δf, and sensed mass, Δm, according to:

$$\Delta m = \frac{\Delta f \times C}{n} \qquad (3.1)$$

where n is the overtone number and C is the mass-sensitivity constant that depends on the thickness (d_q), density (ρ_q), and fundamental frequency (f_0) of the quartz crystal. In principle Eq. (3.1) is only valid for very thin and rigid layers with energy dissipation values close to zero. Its validity can easily be checked as sketched in Figure 3.1, which shows a schematic of an ideal system, since the sensed mass should be independent of the frequency measured at different overtone numbers.

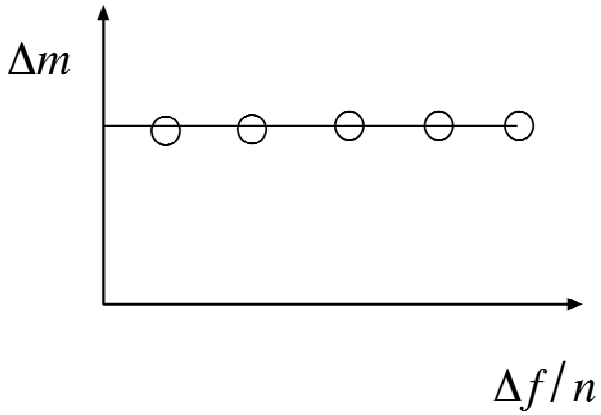

Figure 3.1. *The sensed mass (Δm) calculated from Eq. (3.1) as a function of the frequency (Δf) measured at different overtones (n).*

The Johannsmann model[69] takes into consideration the viscoelastic properties of the film, and their contribution to the sensed mass according to:

$$m_s = m_j\left[1 + J(f)\frac{\rho_f d_f{}^2 4\pi^2 f^2}{3}\right] \qquad (3.2)$$

where ρ_f is the film density, d_f the film thickness, m_s and m_j are the sensed mass calculated from the Sauerbrey and Johannsmann equations, respectively. *J(f)* is the viscoeleastic compliance, which may be frequency dependent. For the adsorption studies on chitosan and SDS adsorption in paper III, we used this model and plotted the Sauerbrey mass, m_s, as a function of frequency squared, f^2, for different overtone numbers and estimated the Johannsmann mass, m_j, from the intercept. Since we found the relation to be linear (see Figure 3.2) we could assume that *J(f)*, which depends on film viscosity and shear modulus, was independent of frequency.

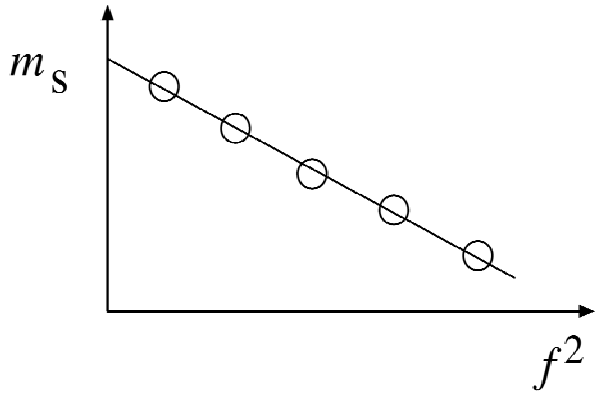

Figure 3.2. *The Sauerbrey sensed mass (m_s) as a function of the frequency squared (f^2) measured at different overtone numbers.*

For the chitosan and heparin multilayer film in paper V the plot between the Sauerbrey sensed mass and the frequency squared, f^2 is not linear, (see the schematic drawing in Figure 3.3). Clearly, *J(f)*, in Eq. (3.2) is frequency dependent. The Voight model[50] was therefore applied to estimate the "true" sensed mass, *m*, for a viscoelastic adsorbed film. A software (Q-tools) provided by the manufacturer (Q-sense) was used to estimate the sensed mass by fitting the measurement data to a Voight model. In the model, changes in frequency, Δf, and energy dissipation, ΔD, are related to the viscoeleastic properties of the film according to equations (3.3-3.5). In brief, the frequency and dissipation change measured at several different overtones are used together with an assumed value of the layer density (ρ_f) to estimate the viscosity (η_f), shear modulus (μ_f), and thickness (d_f) of the adsorbed film.

$$\Delta f = -\frac{1}{2\pi\rho_q d_q}\left(d_f\rho_f\omega - 2d_f\left(\frac{\eta_0}{\delta_0}\right)^2\frac{\eta_f\omega^2}{\mu_f^2+\omega^2\eta_f^2}\right) \qquad (3.3)$$

$$\Delta D = \frac{1}{\pi f\rho_q d_q}\left(2d_f\left(\frac{\eta_0}{\delta_0}\right)^2\frac{\mu_f\omega}{\mu_f^2+\omega^2\eta_f^2}\right) \qquad (3.4)$$

$$m = \rho_f \times d_f \qquad (3.5)$$

where ω ($\omega = 2\pi f$) is the angular frequency of oscillation, η_o is the bulk viscosity, ρ_0 the bulk density, and δ_o ($\delta_o = (2\eta_o\rho_0^{-1}\omega^{-1})^{0.5}$) the viscous penetration depth of the shear wave in the bulk liquid.

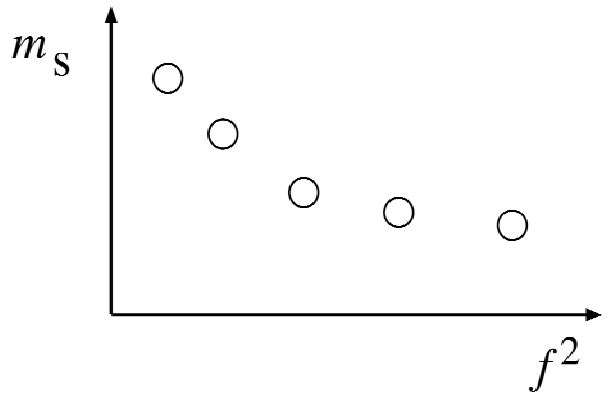

Figure 3.3. *The Sauerbrey sensed mass (m_s) as a function of the frequency squared (f^2) measured at different overtone numbers.*

The Voight model provides a better estimate of the layer properties than the Sauerbrey equation or the simplified Johannsmann model for films showing viscoelastic properties (high ΔD), whereas the drawback is that knowledge of the layer density is needed. However, the model should be used if the measurement data resembles that shown in Figure 3.3. It should be noted that for rigid layers with D close to zero, the Voight model reduces to the Sauerbrey equation.[50]

3.3 Optical methods

Ellipsometry and DPI are optical techniques, used to gain information on the thickness, refractive index, and adsorbed amount, Γ, of an adsorbed film. Contrary to the QCM-D, these techniques estimate the "dry" mass of an adsorbed film. This enables the calculation of the relative solvent content, $w_{solvent}$, and the effective density, ρ_{eff}, of the film by comparing the adsorbed mass obtained by QCM, m_{QCM}, and an optical technique, $\Gamma_{optical}$, according to:

$$w_{solvent}(\%) = \frac{m_{QCM} - \Gamma_{optical}}{m_{QCM}} \times 100 \qquad (3.6)$$

$$\rho_{eff} = \rho_p \frac{\Gamma_{optical}}{m_{QCM}} + \rho_0 \left(1 - \frac{\Gamma_{optical}}{m_{QCM}} \right) \qquad (3.7)$$

where ρ_p and ρ_0 are the bulk densities of the polymer/protein and the background solution, respectively.

3.3.1 Null ellipsometry

The null ellipsometry instruments used were a Rudolph type 436 (Rudolph Research, Fairfield, New Jersey, USA) in paper II, and a Multiskop (Optrel GdBR, Berlin, Germany), in papers III-IV. The same information is obtained from the two instruments.

Ellipsometry measures changes in the polarization of light caused by reflection at an interface. These changes depend on the optical properties of the substrate, the adsorbed film, and the ambient media.[52] By measuring changes in amplitude (Δ) and phase (Ψ) of polarized light upon reflection, the optical properties of the substrate and of an adsorbed film can be calculated. In practical terms this is carried out by numeric iterations of Δ and Ψ using a theoretical four layer model according to Figure 3.4, by assuming that all layers are homogenous and optically isotropic. First, Δ and Ψ were measured for the clean substrate in air and in ambient solution, which enables calculations of the optical properties of the substrate. Once these are determined, the average thickness, d_f, and the average refractive index, n_f, of the adsorbed film can be followed in situ from the measured changes in Δ and Ψ compared to the clean substrate through numeric iterations. A detailed description of these calculations can be found elsewhere.[54,53]

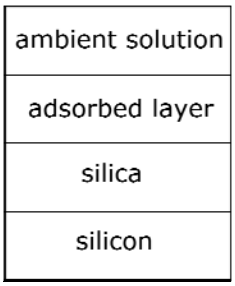

Figure 3.4.*The four-layer optical model used to calculate the thickness and refractive index of an adsorbed layer from ellipsometric data.*

3.3.2 Dual polarization interferometry (DPI)

The DPI used was an AnaLight Bio200 from Farfield Sensors Ltd, UK. The fundamental science of this technique, the instrument, and the details on how the thickness and refractive index were calculated is thoroughly described elsewhere.[55,56] Polarized laser light is focused into two horizontally stacked and separated waveguides, the reference waveguide and the sensing waveguide (see Figure 3.5). The waveguides are composed of silica doped with silicon nitride that confines the laser light within the waveguides due to total internal reflection. By allowing the light from the sensing and reference waveguides to diffract and interfere at the end of the guides, interference fringes (viewing screen) are detected with a CCD camera at some distance away (in the farfield). Adsorption of proteins or polyelectrolytes to the sensing waveguide (viewed as Y symbols in the schematic Figure 3.5) slows down the speed of light whereas it is unaltered in the reference waveguide. This gives rise to a change in the interference pattern. The phase change, $\Delta\phi$, between the reference and sensing waveguide is related to the change in the effective refractive index, N_s of the sensing waveguide according to:[56]

$$\Delta\phi = k_0 L \Delta N_s \qquad (3.8)$$

where k_0 is the free space wavenumber and L is the interaction length. Two different polarization modes (polarization 1 and 2, that are parallel and perpendicular to the surface) are used in the measurement that results in two independent N_s values. Each N_s value satisfies a large number of thickness and refractive index combinations as seen in Figure 3.5. However, only one thickness, d_f, and refractive index, n_f, of the adsorbed layer satisfy the conditions for both polarization modes.

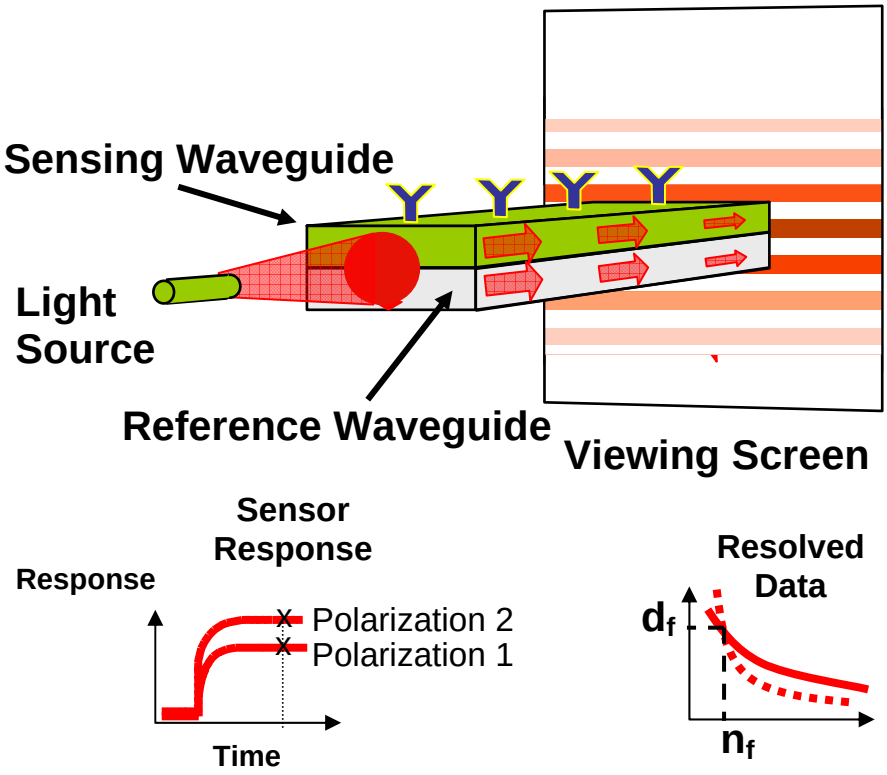

Figure 3.5. *A schematic presentation of the DPI technique. Printed with permission from Farfield Sensors Ltd, UK.*

3.3.3 Adsorbed amount

The n_f and d_f values obtained from ellipsometry or DPI were used to calculate the adsorbed amount, Γ, using the de Feijter[70] or Cuypers[71] equation. However, a problematic situation arises for adsorbed layers consisting of several materials with different optical properties. Especially, in paper III the refractive index increment, *dn/dc*, is different for pure chitosan (0.18) and SDS (0.12) and the value for complexes formed by chitosan and SDS is unknown. The de Feijter equation Eq. (3.9), where n_0 is the refractive index of the ambient, shows that this difference in *dn/dc* can induce a large uncertainty in the calculated adsorbed amount.

$$\Gamma = \frac{d_f (n_f - n_0)}{dn/dc} \qquad (3.9)$$

This subject is thoroughly described in paper III and in the PhD-thesis by Lubica Macakova, KTH.[72,73] For composite layers, the highest *dn/dc* value was used throughout this thesis with the knowledge that this will correspond to the lowest estimate of the adsorbed amount for a given layer.

3.4 Fluorescence methods

The fluorescence methods are all based on a three step process illustrated by a Jablonski diagram in Figure 3.6 (left).[59] A fluorescence molecule is excited, *hv*(Ex), with an external light source (e.g. laser), by absorption of energy, to a higher electronic state (S1'). In the higher energy state the molecule interacts with its environment that results in relaxation to a lower energy state (S1) due to energy dissipation. By emitting energy, *hv*(Em) the molecule returns to its ground state (S0). Generally, the emission intensity is recorded (photon counter), which provides information on the amount of dye molecules. The wavelength of the laser light is set to the absorption maxima of the fluorescent molecule and the emission intensity is measured at the wavelength for its emission maxima. This is depicted in Figure 3.6 (right), where the energy of fluorescence emission (longer wavelength) is always less than the absorbed energy due to the energy loss in the excited state.

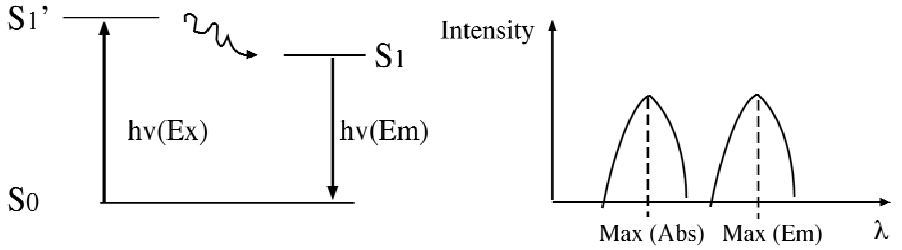

Figure 3.6. *An illustration of the absorption, excitation, and emission of light by a fluorescence molecule shown as a Jablonski diagram (left) and as intensity versus wavelength (right).*

3.4.1 Total internal reflection fluorescence (TIRF)

TIRF is an optical method capable of detecting fluorescent molecules adsorbed at or in the vicinity of a solid interface.[57] The instrument used in paper IV was built at YKI, (Sweden), and has been thoroughly described by Lassen and Malmsten.[58] In paper VI, TIRF measurements were carried out with a modular Spex-Fluorolog-3 fluorescence spectrometer (Horiba Jobin Yvon, Edison, NJ, USA). The latter instrument set-up is superior in that it

can measure the emission intensity at several wavelengths simultaneously (which is required for FRET measurements, section 3.4.2).

Figure 3.7 shows a schematic of the TIRF technique, where incident light is fully reflected from the interface between two media of different optical density (refractive index), where $n_1 > n_2$. In this work media 1 was a quartz glass substrate (n_1 = 1.46-1.47) and media 2 was either a protein or polymer solution ($n_2 \approx 1.34$). At the interface, an evanescent wave penetrates into the medium of lower refractive index (protein/polymer solution). The dye molecules, bound to a polymer (paper VI) or protein (paper IV), that are within the evanescent field (< 200 nm from the interface in this case) will absorb energy and become excited. The fluorescence emission intensity was measured by the detector (photon counter).

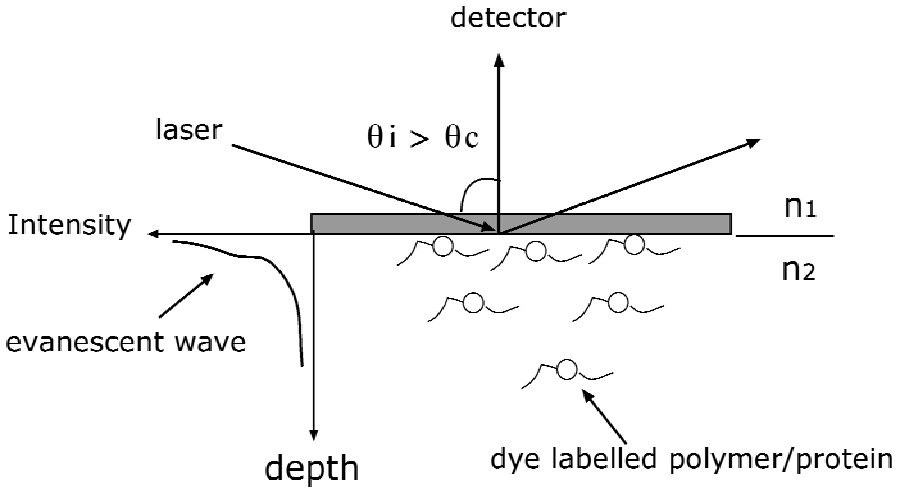

Figure 3.7. *A schematic of the TIRF technique.*

A few conditions have to be fulfilled for the technique to work properly. Total reflection only occurs if n_1 is larger than n_2 and the angle of incidence θ_i exceed the critical angle θ_c, calculated from Snell's law*:*

$$\theta_c = \sin^{-1}(n_1 / n_2) \qquad (3.10)$$

Further, the wavelength of the laser must coincide with the absorbance region of the particular dye used and preferentially be close to its maximum absorbance wavelength (see Figure 3.6).

3.4.2 Fluorescence resonance energy transfer (FRET)

The FRET technique is based on the energy transfer between two fluorophores. The same instrument and theory is used for FRET as for TIRF, with the exception that two different fluorophores are required for FRET. These two are referred to as donor dye and acceptor dye, where the donor dye always has absorption maxima at shorter wavelengths than the acceptor dye. The donor dye in its excited state may transfer energy through dipole-dipole interactions to an acceptor dye in close proximity (1-10 nm). Figure 3.8 shows an illustration of the FRET process where the dyes are close enough (top in Figure 3.8) or too far apart (bottom in Figure 3.8) for transfer of energy to occur. Experimentally, FRET is observed as a decrease in emission intensity of the donor emission and an increase in acceptor emission intensity when the system is excited at the donor excitation wavelength. The efficiency of this transfer decreases with the 6th power of the dye separation distance Eq. (3.11), and if a sufficient distance separates the dyes there is no change in the donor emission intensity caused by the presence of the acceptor dye. The relation between energy transfer efficiency, E, and the donor-acceptor dye separation, r, is given by:[59]

$$E = \frac{1}{1+\left(r/R_0\right)^6} \tag{3.11}$$

where R_0 is the Förster radius at which E is 50 % for a specific dye pair. The efficiency of energy transfer is calculated from exciting the system with the donor excitation wavelength and measuring the donor emission intensity in the presence, F_{da}, and in the absence, F_d, of the acceptor dye.[59]

$$E = 1 - \frac{F_{da}}{F_d} \tag{3.12}$$

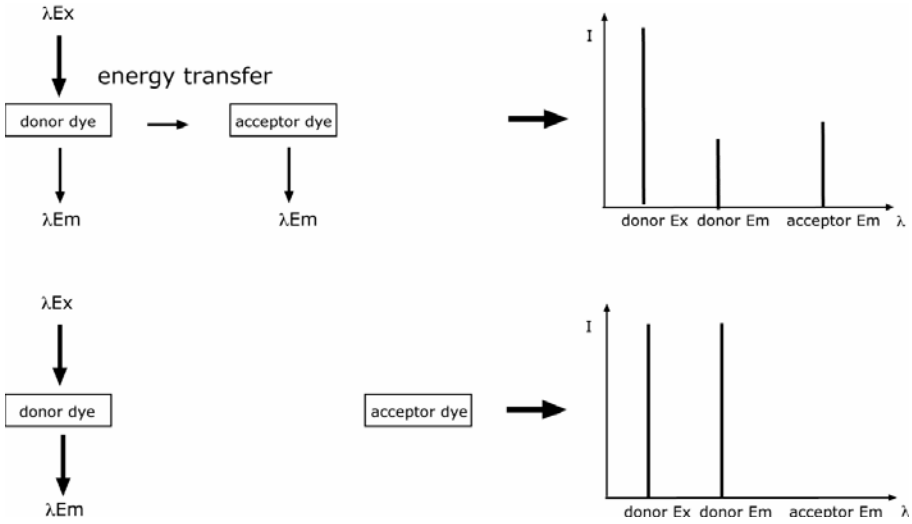

Figure 3.8. *A schematic of the FRET technique and the experimentally measured changes in emission (Em) intensity (I) from the donor and acceptor dyes depending on whether or not energy transfer occurs.*

3.5 Surface Force Apparatus (SFA)

Interactions between biopolymer-coated surfaces were investigated using the MARK-IV[74] SFA (Anutech, Australia) in papers I-II. With this technique the total force acting between two macroscopic molecularly smooth surfaces in a crossed cylinder configuration is measured as a function of surface separation. A schematic of the technique is shown in Figure 3.9. In brief, SFA provides information on surface forces, layer thickness (extended and compressed) and layer compressibility. In this technique two surfaces are used, mica sheets glued onto silica disks with a silver coating facing the disk. One surface is mounted on a cantilever spring and the other surface is mounted on a piezoelectric crystal, which is used to change the separation between the two mica surfaces. The surface separation is obtained by optical interferometry using a white-light source and analyzing the fringes of equal chromatic order (FECO) when surfaces are in contact and far apart. During each force-distance measurement, the movement of the piezo is calibrated at large separations where no force acts between the surfaces. This also corresponds to the change in surface separations (ΔD). At smaller separations, where the surfaces interact, the change in surface separation will be different from that when no interaction is present, at a given change in piezo-voltage (ΔD_0). This difference is due to deflection of the cantilever spring. The force, F, is then calculated from Hook's law:

$$F = k(\Delta D - \Delta D_0) \qquad (3.13)$$

where k is the spring constant. The resolution in surface separation is about 1-2 Å while the resolution in the force, normalized with the local radius of the interacting surfaces, is approximately 10 μN/m.

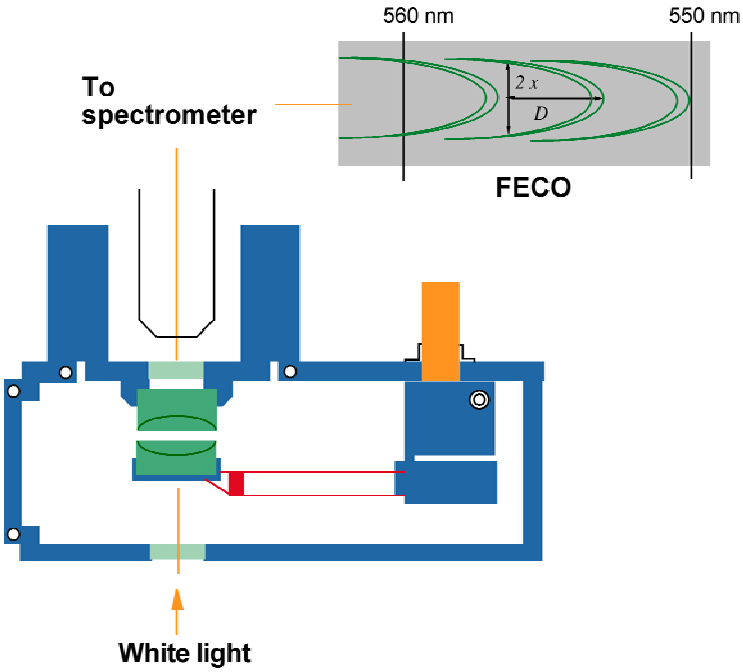

Figure 3.9*. A schematic of the SFA technique kindly provided by Eva Blomberg.*

3.6 X-ray-photoelectron Spectroscopy (XPS)

XPS was used in paper I to provide the relative amounts of different elements, (mainly nitrogen and carbon) in protein layers adsorbed on mica surfaces. A detailed description of the instrument, Kratos AXIS HS X-ray photoelectron spectrometer (Kratos Analytical, Manchester, UK), is provided by Rojas et al.[75] The number of nitrogen atoms per unit area was determined by comparing the N1s peak from the adsorbed protein with the K2p peak for the mica substrate following the method developed by Herder et al.[76]

3.7 Materials and Substrates

The main materials and substrates used in this work and their characteristics are briefly summarized in Table 3.2 and Table 3.3, respectively. A more detailed description can be found in sections 3.7.1 and 3.7.2.

Table 3.2. *Brief description of the physical properties of the chemicals used in this work.*

	Source	Type	M_w (kDa)	Charge (sign)	Main ionization groups	iep
Chitosan	Crab shells	Linear polysaccharide	150	positive	amine (pKa = 6-6.5)	-
Heparin	porcine intestinal mucosa	Linear polysaccharide	14	negative	Sulfate (pKa = 1) and Carboxyl (pKa ~3)	-
SDS	synthetic	Anionic surfactant	0.288	negative	Sulfate (pKa = 1)	-
Lysozyme	hen egg white	Hard globular protein	14.1	net positive	-	pH 11
β-casein	bovine milk	Flexible protein	24	net negative	-	pH 5.2
Mucin (further purified)	bovine submaxillary gland	Linear Flexible glycoprotein	2900	net negative	sialic acid (pKa ≈ 2.6) and sulfate (pKa ≈ 1)	-
Mucin (as received)	bovine submaxillary gland	Linear Flexible glycoprotein	7000	net negative	sialic acid (pKa ≈ 2.6) and sulfate (pKa ≈ 1)	-
Albumin	Bovine serum	Soft globular protein	66	net negative		pH 4.7

3.7.1 Proteins

Mucins are large glycoproteins (M_w > 1 MDa) with important functions in the mucous, which covers the epithelial cell surfaces. Its function is to lubricate the surface by binding water and to prevent non-specific interactions of cells and proteins. The carbohydrate content is large, constituting approximately 80 % of the total mass of mucin. Further, it contains a large amount of sialic acid (pKa ≈ 2.6) and sulfate groups (pKa ≈ 1) that makes mucin highly negatively charged at most solution pHs. In this work bovine submaxillary gland mucin, BSM (Sigma M3895), was used either as received (paper III) and/or further purified (paper I). The purification step reduces the average M_w from approximately 7 MDa[77] to 2.9 MDa[78], whereas the sialic content is increased from 12 wt-% to 36 wt-%.[78]

Bovine serum albumin (BSA) is a soft (low conformational stability) globular protein with a molecular weight of 66 kDa and an isoelectric point of 4.7.[79] Its structure is similar to the triangular shape (80x80x3 nm^3) of human serum album as estimated by X-ray crystallography.[80] The BSA used in this work was extracted from the Sigma BSM (M3895).[78]

Lysozyme is a hard globular protein present in tears, saliva, and egg white. It is an enzyme which causes the hydrolysis of bacterial cell walls and constitutes a defence mechanism against bacterial infections.[81] The lysozyme used in this work was obtained from hen egg white (Sigma-Aldrich, L6876). It has an ellipsoidal structure with dimensions of 45x30x30 Å, and a molecular weight of 14.1 kDa.[81] The isoelectric point of lysozyme is approximately 11, and at the pH used in this work (pH 8.5) it has a net charge close to +8.[82]

β-casein is a flexible protein present in milk, where its function is to act as an electric and steric barrier against fat coalescence.[83] The molecular weight is approximately 24 kDa with an isoelectric point of 4.6 and a net charge of -15 at pH 7.[84] It is therefore net negatively charged at pH 8.5, which was the pH used in this work. The β-casein (from bovine milk) was received from Hannah Research Institute, Scotland.

3.7.2 Polysaccharides

There are many different classes of polyelectrolytes out of which charged polysaccharides are one. The name polysaccharide refers to the sugar based (saccharide) repeat unit, which makes the polysaccharides less flexible in comparison to most linear synthetic polyelectrolytes.

Chitosan is a natural polysaccharide derived by alkaline deacetylation of chitin, which is a polymer found in shellfish. Both chitosan and chitin consist of N-acetyl-glucosamine and N-glucosamine, but when the number of N-glucose units is higher than 50 % the polymer is termed chitosan. The structure of chitosan is shown in Figure 3.10. It is a weak polyelectrolyte since its charge depends on the solution pH (pKa = 6-6.5). In this work chitosan from crab shells was used (Fluka, cat. No. 50494 or 22741). Chitosan has a rather high intrinsic stiffness due to the saccharide units, with a persistence length of 4 nm. The degree of deacteylation for the chitosan used in this study was 85-90 % and the persistence length was approximately 6 nm at pH 4, where the polymer is highly charged.[85,72] The polysaccharide is widely used in biomedical applications, such as drug formulations and antibacterial treatment, due to its biocompatibility, biodegradability, and antibacterial properties.[86,87]

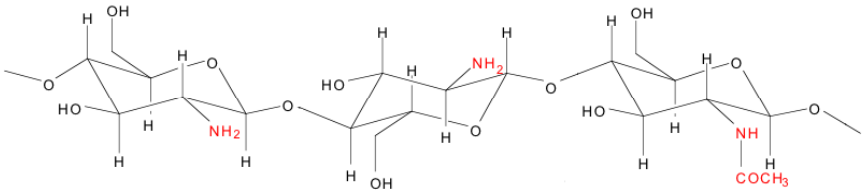

Figure 3.10. *The molecular structure of chitosan.*

Heparin is an anionic polysaccharide isolated from animal tissues that belong to the glucoaminoglycan family. Heparin is highly sulfated, which together with its carboxyl groups renders it highly negatively charged in solution above pH 1. It is heterogeneous in size and composition but the sequence shown in Figure 3.11 accounts for more than 80 % of the molecules.[88] A radius of gyration of 4.2 nm has been estimated from SAXS measurements in 0.2 M NaCl and a molecular weight equal to that used in this study, 14 kDa.[88] Due to the unique 3-sulfated $GlcNSO_3$ in some of the chains, it possesses anticoagulant activity and it has been used for nearly 40 years in medicine and surgery, i.e. heart-lung machines and artificial kidneys to avoid blood clotting.[89] Heparin from porcine intestinal mucosa was obtained from Merck Bioscience (cat. No. 375095).

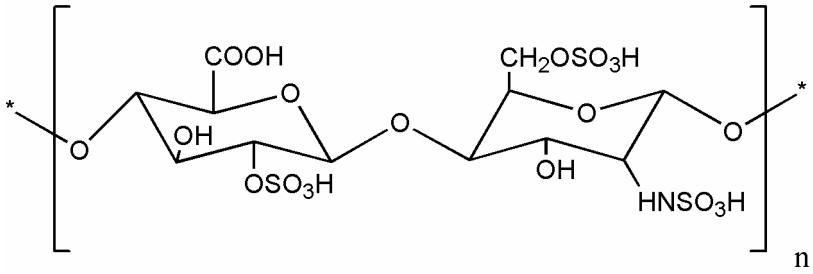

Figure 3.11. *Structure of the major repeat unit in heparin, showing the four ionisable groups, three sulfate and one carboxyl per disaccharide unit.*

3.7.3 Substrates

Adsorption studies were mainly carried out on negatively charged hydrophilic substrates such as mica, silica or glass. The reason for using slightly different substrates was due to instrumental requirements. The cleaning procedure of the substrate surfaces varied between the different experimental techniques. However, it is important to note that all substrates become highly negatively charged and hydrophilic after cleaning, with contact angles less than 10°.

Table 3.3. *An overview of the substrates used in this work.*

Method	***Substrate***	***Cleaning*** [a)]	***Surface potential*** [b)]	***Contact angle*** [c)]
QCM-D and AFM	Quartz crystals covered with silica (oxide layer 50 nm)	Alkaline surfactant solution	Negative	< 10°
DPI	Silica waveguides doped with nitrogen	Acid/methanol solution and alkaline surfactant solution	Negative	< 10°
Ellipsometry	Silicon slides covered with silica (oxide layer ~30 nm)	Alkaline surfactant solution or acid and base	Negative -45 mV[90, d)]	< 10°
TIRF, FRET	Quartz glass	Alkaline surfactant solution or acid and base	Negative	< 10°
SFA and XPS	Mica	Freshly cleaved	Negative -85 to -100 mV[91]	< 10°

a) For details of the cleaning procedure the readers are referred to the appended papers.

b) For the silica and glass surfaces the charge originates from silanol surface groups. The negative charge of the mica originates from isomorphous substitution of Si^{4+} for Al^{3+} in the mica crystal.[91]

c) After the cleaning procedure the surfaces were completely wetted by water and the advancing contact angle was very difficult to measure accurately.

d) Measured at pH 7.0 and 1 mM NaCl. The magnitude of the charge increases with increasing pH and ionic strength due to dissociation of the silanol groups.[92, 93] The isoelectric point (iep) of silica is at approximately pH 2.[94]

4 Summary of Key Results

This section summarizes the results that were particularly interesting in this work. For a full coverage of all results, the reader is referred to the included papers, attached at the end of the thesis.

4.1 Adsorption of mucin (BSM) depending on its purity

The main goal in paper I was to understand how impurities of small proteins, particularly bovine serum albumin (BSA), present in bovine submaxilary mucin (BSM) preparations influence the adsorption and layer structure of BSM on negatively charged hydrophilic surfaces. Our interest stems from a previous finding that as received commercial BSM (Sigma, M3895) contains up to 9 wt-% of albumin (BSA).[95] However, BSA could be eliminated after additional purification, resulting in a pure BSM product, which in the following is referred to as purified BSM.[95] The surface force apparatus (SFA) was used to obtain information about the layer structure of adsorbed as received BSM, purified BSM, pure BSA, and pre-equilibrated mixtures of purified BSM and BSA on mica. The force curves, in Figures 4.1-4.2 also include schematic drawings showing our interpretation of the unperturbed layer structure prior to compression.

4.1.1 As received versus purified BSM

The force measured between two mica surfaces pre-coated with as received BSM and purified BSM across a PBS buffer solution (at pH 7.4 and ionic strength 150 mM) is shown in Figure 4.1. The force measured between the uncoated mica surfaces in the buffer solution is shown as a solid line in Figure 4.1a, where a repulsive electrostatic double layer force is seen at surface separations below 40 Å. When the BSM-coated surfaces are moved towards each other, a steric force begins at approximately 300-500 Å. This distance indicates that the length of the extended layer is 150-250 Å on each mica surface. The extended layer, which we suggest contains a large number of loops and tails (see schematics), is compressed into a very thin film. The tails and loops are irreversibly compressed, on the time scale of the measurement, since there is a hysteresis in the force profile between compression and decompression (open symbols). The thin compressed layers and the high compressibility are a result of low BSM chain density on mica due to that, in the solution conditions used, both mica and BSM molecules are highly negatively charged.

By comparing the compressed layer thickness of the layer adsorbed from purified BSM (10 Å per surface, Figure 4.1a) with that adsorbed from as

received BSM (35 Å per surface, Figure 4.1b), it was found that the purified BSM compressed into a significantly thinner layer. The discrepancy indicates that the layer adsorbed from as received BSM probably contained impurities e.g. BSA.

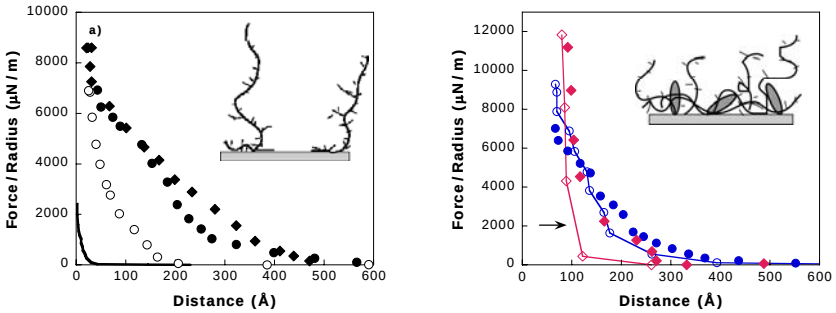

Figure 4.1. *The force as a function of surface separation between two mica surfaces uncoated (solid line) or pre-coated with purified BSM across a PBS buffer solution is shown in Figure a) for two separate measurements (circles and diamonds). In Figure b), the mica surfaces were pre-coated with a protein layer adsorbed from as received BSM (red diamonds) or a pre-equilibrated BSM-BSA mixture with 9 wt-% BSA (blue circles). Filled and unfilled symbols represent the force measured on approach and separation, respectively. The Schematics show our interpretation of the unperturbed layer structure prior to compression.*

4.1.2 Pre-equilibrated fractions of BSM and BSA

In Figure 4.1b, the force profiles of layers adsorbed from as received BSM or a pre-equilibrated BSM-BSA mixture with 9 wt-% BSA are shown. In terms of compressed layer thickness these layers are very similar. However, the force profiles display a different structure since only the layer adsorbed from as received BSM shows a hysteresis in the measured force between compression and decompression (marked with an arrow in Figure 4.1b). An increased fraction of BSA to BSM in the deposition solution (50 wt-% BSA) results in a considerably thicker adsorbed layer (Figure 4.2).

The small difference between extended and compressed layer thickness reflects a dense layer structure, consistent with the rigid structure of adsorbed BSM-BSA complexes on polystyrene surfaces as previously reported by Feiler et al.[96] Further, the layer adsorbed from the BSM-BSA mixture (50 wt-% BSA) is significantly thicker than that formed after adsorption of pure BSA (Figure 4.2).

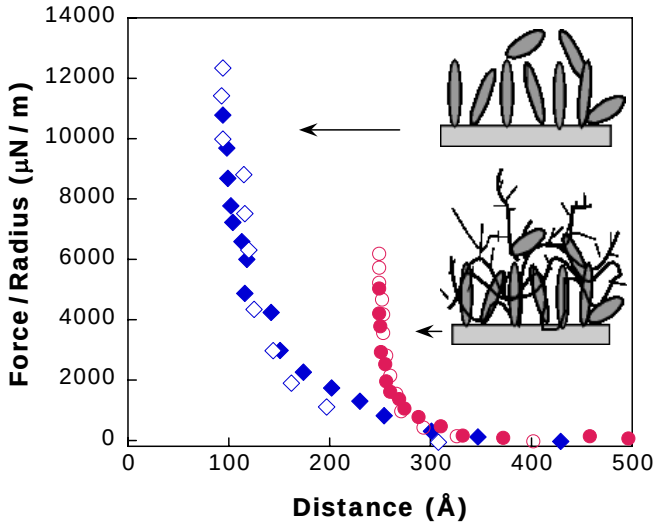

Figure 4.2. *The force as a function of surface separation between two mica surfaces pre-coated with BSA (blue diamonds) and a pre-equilibrated BSM-BSA mixture having 50 wt-% BSA (red circles) across a PBS buffer solution. Filled and unfilled symbols represent the force measured on approach and separation, respectively. The Schematics show our interpretation of the unperturbed layer structure prior to compression.*

Complementary results obtained with X-ray photoelectron spectroscopy (XPS) show that the chemical composition of layers adsorbed from BSA or the BSM-BSA mixed solution (50 wt-% BSA) is identical (Table 4.1). Thus, BSA is the dominant species in mixed BSA-BSM layers adsorbed from 1:1 mixtures of BSA and BSM. However, from Figure 4.2 it is evident that the small amount of BSM in the layer significantly affects its final layer structure. Further, the chemical composition (number of nitrogen atoms) for layers adsorbed from the BSM-BSA solution having a 5 wt-% BSA is higher, but approaches, the one obtained from as received BSM, see Table 4.1. Hence, the difference in the force profiles between as received BSM and the pre-equilibrated BSM-BSA mixture (9 wt-% BSA), in Figure 4.1b, can be explained by a higher BSA content in the BSM-BSA solution, which results in a more compact layer with a lower fraction of extended loops and tails. Thus, it is of great importance to characterize the mucin used, since differences in purity resulted in very different adsorption behaviours of

BSM in terms of adsorbed amount and layer structure. The presence of BSA impurities altered the adsorption of BSM significantly.

Table 4.1. *X-ray photoelectron spectroscopy analysis of protein-coated mica surfaces, showing the number of nitrogen atoms per* cm^2 *and the carbon content in protein layers relative the bare mica surface. The maximum and minimum values reported are due to that three independent measurements were carried out on pure mica surfaces.*

Adsorption of:	***No. of Nitrogens/*** cm^2	$Area(C)_{protein}/Area(C)_{mica}$
BSM (as received)	$(1.35\text{-}1.44)\times10^{14}$	1.2-1.3
BSM (purified)	$(3.6\text{-}3.9)\times10^{13}$	1.0-1.1
BSA	$(1.2\text{-}1.3)\times10^{15}$	3.4-3.8
BSM:BSA (50 wt-% BSA)	$(1.2\text{-}1.3)\times10^{15}$	3.4-3.8
BSM:BSA (9 wt-% BSA)	$(3.0\text{-}3.2)\times10^{14}$	1.5-1.7
BSM:BSA (5 wt-% BSA)	$(2.2\text{-}2.3)\times10^{14}$	1.3-1.5

4.1.3 Driving force for adsorption of BSM and BSA

Many proteins are known to adsorb to negatively charged surfaces from solutions having pH-values above their isoelectric point (iep) even though, the protein and the surface have the same sign on their net charge. The driving force for globular proteins (such as albumin) has been suggested to origin mainly from structural rearrangements within the protein upon adsorption.[11, 79] The gain in entropy upon BSA adsorption then overcomes the electrostatic repulsion, especially at sufficiently high salt concentration due to screening. This explains the relatively thick BSA layer adsorbed on mica in Figure 4.2.

In paper I and II, we suggested that the adsorption of BSM to mica surfaces is driven mainly by the electrostatic attraction between positively charged patches on BSM and the negatively charged mica surface even though BSM is net negatively charged. There are mainly two findings, which makes us believe that this adsorption is driven by electrostatics: Lindh *et al*. showed that an increased salt concentration enhanced the adsorption of BSM to negatively charged surfaces due to the decreased BSM-surface charge repulsion.[16] Further, Feldötö *et al*. showed that substantially more BSM

adsorbed on a negatively charged hydrophilic surface than on a hydrophilic uncharged surface.[20] The extended BSM conformation on mica with loops and tails and the pure repulsion observed upon compression/decompression in Figure 4.1 is then a consequence of the electrostatic repulsion. For the adsorption of BSM-BSA complexes it is important to note that the BSM and BSA forms complexes already in the pre-equilibrated mixed solution, which then adsorbs onto the substrate. It has been shown previously that BSM does not adsorb onto a BSA layer pre-adsorbed on polystyrene (PS) surfaces, whereas BSA adsorbed onto a pre-adsorbed BSM layer.[96] Further, in line with our findings a substantial amount of BSM-BSA complexes adsorbed on PS. However, the PS surface is not only negatively charged but also hydrophobic, and the hydrophobic interaction is probably the major driving force for adsorption of BSM-BSA complexes to the substrate.

4.2 Interactions between SDS and pre-adsorbed BSM on silica

The adsorption studies with BSM on negatively charged hydrophilic surfaces in paper II were carried out with the as received BSM used in paper I. In order to compare our results with those in a previous report[17], the BSM solution deposition conditions (a 30 mM NaCl solution at pH 5.8) were different from that used in paper I. The ellipsometry measurement in Figure 4.3 shows that the net negatively charged BSM adsorbs to the negatively charged silica substrate in line with that observed on mica in Figure 4.1. The adsorbed amount is only slightly decreased upon rinsing with a polymer-free background solution. Addition of SDS with a surfactant concentration equal to 3.3 mM (1 cmc SDS in 30 mM NaCl) results in desorption of 80 % of the pre-adsorbed mucin. It should be noted that SDS has no affinity for silica and hence desorption is not due to a competitive process between BSM and SDS for the silica substrate.[72,97] The interaction between SDS and pre-adsorbed BSM on negatively charged hydrophilic surfaces is mainly of hydrophobic origin, as also suggested in previous reports.[17,77] Desorption of BSM-SDS complexes results from an increased repulsion between the negatively charged substrate and the higher negatively charge of BSM-SDS complexes compared to BSM alone. This well known finding is actually affecting us in our daily life routines, since mucins are important for hydration[14] and lubrication[98,99,100] in the oral cavity (mucosa) and most personal care products such as toothpaste contain SDS. As a result, some people get a dry mouth feeling after brushing their teeth with toothpaste, and it can be a severe problem for those having an impaired saliva production.

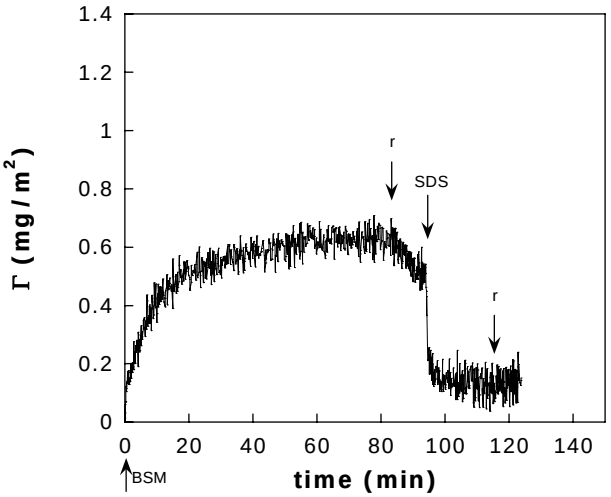

Figure 4.3. *The adsorption of BSM on silica as a function of time. After about 80 min the surface is rinsed with the background solution, r, and then by SDS, and finally with the background solution again. The concentration of SDS was 1 cmc, which is equal to 3.3 mM in the 30 mM NaCl background solution. Measurements were carried out with the ellipsometry technique.*

4.3 Interactions between SDS and preadsorbed BSM-chitosan complexes on silica

In order to prevent BSM desorption by SDS, we investigated the possibility of using a protective layer of the natural cationic polysaccharide, chitosan, adsorbed onto the pre-adsorbed BSM layer. The average film thickness of the BSM layer on silica is relatively large (34 nm), and the very low refractive index of 1.346 is similar to the one of the background electrolyte solution (1.343) in Figure 4.4. Thus, these characteristics are in line with the extended and highly compressible BSM layer adsorbed on mica, as observed in paper I (Figure 4.1). Clearly, BSM layers contain large amounts of solvent. In Figure 4.4 it is shown that adsorption of chitosan results in a very small increase in the adsorbed amount (0.1 mg/m^2) and layer refractive index, whereas a significant decrease is observed in the layer thickness. This indicates that adsorption of chitosan induces a significant compaction. The adsorbed amount increases further upon addition of SDS but the binding between SDS and BSM-chitosan complexes is weak since most of the SDS

can be rinsed off by the background solution. Clearly the BSM-chitosan complexes resist desorption by SDS. However, recently it has been shown that the layer compaction induced by adsorption of chitosan (in Figure 4.4b) reduces the lubrication properties of the BSM film.[99] This could result in a dry mouth feeling, similar to that induced on BSM by exposure to SDS. However, it is important to note that even though mucins are the major protein constituents of mucous, other proteins such as albumin, lysozyme, lactoferrin, and IgG associate with mucins in the native mucous.[101] As observed in section 4.1, the BSM layers containing BSA has a less extended structure compared to those containing only BSM. As a consequence, chitosan adsorption to a mucous film does not necessarily induce such a severe layer compaction as observed here.

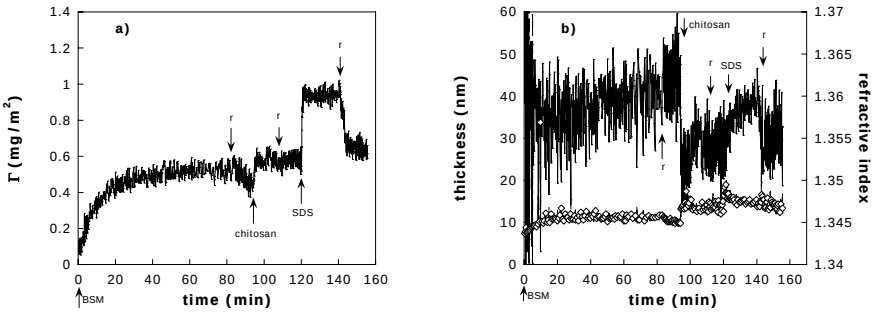

Figure 4.4. *The evolution in ellipsometric adsorbed amount (a), layer thickness (line) and refractive index (diamonds) (b) of a BSM layer adsorbing on silica, followed by adsorption of chitosan and SDS. Every adsorption step is followed by rinsing, r, with the background electrolyte solution (30 mM NaCl). The concentration of SDS was 1 cmc, which is equal to 3.3 mM in the electrolyte solution.*

4.4 Interactions between SDS and preadsorbed chitosan on silica

The seemingly weak interactions between BSM-chitosan layers and SDS lead us to further explore the interaction between SDS and chitosan in more detail. In paper III, the interactions between chitosan and SDS were investigated at the solid-liquid interface and in bulk solution with particular emphasis on the effect of solution ionic strength. For this purpose several different measurement techniques were used in order to follow the chitosan-SDS association at the air-liquid interface, bulk phase, and at the low charged silica substrate at pH 4. This section deals exclusively with the silica-chitosan and silica-chitosan-SDS interactions, and the interested reader is referred to paper III for a description of the chitosan-SDS interactions in bulk solution and at the air-liquid interface.

4.4.1 Adsorption of chitosan on silica surfaces

The electrostatic interactions, such as the surface-chitosan attraction and the inter/intra molecular electrostatic repulsion of chitosan can be altered by changes in solution ionic strength. Figure 4.5a shows the ellipsometric adsorbed amount, Γ_{Ellips}, and thickness, d_{Ellips}, of chitosan layers adsorbed on silica from solutions with a $NaNO_3$ concentration ranging from 0.1 mM to 500 mM. The increase in $NaNO_3$ concentration from 0.1 mM to 30 mM resulted in a significant increase in both Γ_{Ellips} (from 0.1 mg/m^2 to 0.14 mg/m^2) and d_{Ellips} (from 0.5 nm to 2 nm), whereas these changes were in comparison small upon further increasing the ionic strength in the interval 30-500 mM. Further, no adsorption of chitosan to silica was detected at 1000 mM. This dependence on solution ionic strength suggests that the major driving force for chitosan adsorption on silica at pH 4 is the electrostatic attraction. At this pH chitosan is highly positively charged due to its many protonated amine groups, whereas silica has a low negative charge density (iep = 2).[94] The electrostatic attractions can occur due to a polymer-induced dissociation of surface silanol groups as suggested by Shubin and Linse.[102] The increased ionic strength induces screening of the charges along the chitosan chains and the polymer adopts a more coiled structure, resulting in thicker layers and higher adsorbed amounts. However, the electrostatic attraction between chitosan and the oppositely charged substrate is also screened by salt and at sufficiently high ionic strength (1000 mM) no adsorption occurs.

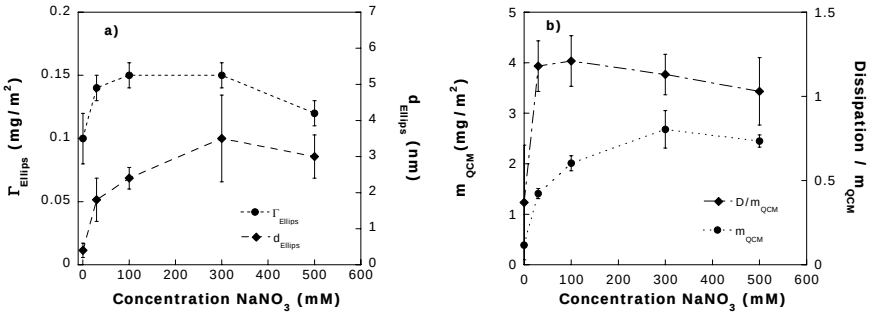

Figure 4.5. *The adsorbed amount (Γ_{Ellips}) and thickness (d_{Ellips}) measured with ellipsometry (a) and the sensed mass (m_{QCM}) and layer dissipation per unit sensed mass (D/m_{QCM}) obtained with QCM-D (b) is shown for an adsorbed chitosan layer on silica as a function of the deposition solution $NaNO_3$ concentration. Error bars indicate the standard deviation between three independent measurements.*

The same measurements carried out with the QCM-D technique shows essentially the same evolution in chitosan sensed mass, m_{QCM}, as a function of solution ionic strength (Figure 4.5b). The major difference is that the sensed mass is considerably higher than the adsorbed amount. This is due to that ellipsometry measures the "dry" adsorbed amount whereas QCM-D measures the sensed mass, which also includes the trapped/bound solvent in an adsorbed layer. From the difference, we estimated the relative solvent content from Eq. (3.6) to on average 75 wt-% and 90-95 wt-% in layers adsorbed from a 0.1 mM and ≥ 30 mM solution, respectively. The QCM-D technique also provides information of the layer structure, which is shown as the energy dissipation per unit sensed mass, D/m_{QCM}, in Figure 4.5b. At 0.1 mM the layer is rigid (low D/m_{QCM}), whereas layers adsorbed from solutions at or above 30 mM are more dissipative. The high water content in all films and the low water content dependence on changes in film thickness and in layer rigidity is unexpected. This is suggested to be caused by the incomplete substrate coverage of chitosan, which is 15 % for the highest adsorbed amount 0.15 mg/m^2, if we assume an area of 25 Å^2 per glucoside ring.[103] The "patchy" adsorbed layers are rough in the nanoscale range, which results in that a large part of the solvent is mechanically trapped in-between polymer molecules and thus oscillates with the QCM crystal.[104] This is reasonable since the solvent content (75-95 wt-%) is similar to the percentage of uncovered substrate area.

A comparison of the adsorption of chitosan on low charged silica (Figure 4.5) with that previously reported on highly charged mica when using identical solution conditions, shows a ten times higher chitosan adsorbed amount on mica.[105] However, the layer response to solution ionic strength was similar, with thicker layers being formed at higher ionic strength. In paper V, chitosan adsorption studies were carried out on silica surfaces at solution pH 5.8 and pH 4.2, using the QCM-D and dual polarization interferometry (DPI) techniques. The electrolyte concentration was either 30 or 150 mM NaCl in these measurements. The results from that study (paper V) are summarized in Table 4.2 together with some of the values obtained from Figure 4.5. Both the adsorbed amount and sensed mass increase when the solution deposition pH is raised from pH 4.2 to pH 5.8. This is reasonable since silica has a higher charge density at pH 5.8 compared to pH 4.2 and the fact that chitosan molecules are less charged at 5.8 (pka = 6-6.5)[106]. As a consequence, more chitosan molecules have to adsorb in order to compensate for the higher surface charge of silica at pH 5.8. However, the layer structures are similar, independent of solution pH, since the dissipation per unit sensed mass is, within experimental errors, almost the same.

Table 4.2. *A summary of the results on chitosan adsorption on silica surfaces at various solution deposition conditions measured with ellipsometry, DPI, and QCM-D.*

	pH 4.0	***pH 4.2***	***pH 4.0***			***pH 5.8***			
Ionic strength (mM)	**Γ_{Ellips} (mg/m^2)**	**Γ_{DPI} (mg/m^2)**	**Γ_{QCM} (mg/m^2)**	**D/Γ_{QCM}**	**Water (%)**	**Γ_{DPI} (mg/m^2)**	**Γ_{QCM} (mg/m^2)**	**D/Γ_{QCM} (mg/m^2)**	**Water (%)**
30	0.14	≤ 0.1	1.4±0.1	1.2±0.1	90±2	0.54±0.07	2.8±0.3	0.9±0.1	80±4
100	0.15	-	2.0±0.2	1.2±0.15	93±2	-	-	-	-
150	-	0.15±0.05	2.0±0.7	1.4±1.0	90±9	0.61±0.03	3.5±0.4	0.9±0.3	82±3
300	0.15	-	2.7±0.4	1.1±0.1	94±2	-	-	-	-

4.4.2 Interactions between SDS and pre-adsorbed chitosan

Figure 4.6 shows the interactions between SDS and preadsorbed chitosan on silica surfaces in 0.1 mM $NaNO_3$ and 30 mM $NaNO_3$ at pH 4.0. By comparing the QCM-D results in Figure 4.6 c-d, it was found that the response of chitosan layers on silica to addition of SDS was highly dependent on the structure of the initial chitosan layer on silica. In 30 mM (Figure 4.6 d) the relatively thick and extended chitosan layer was collapsed by addition of SDS, whereas the collapse was insignificant in 0.1 mM (Figure 4.6 c). The collapse in 30 mM occurred already at the lowest surfactant concentration investigated, 0.02 cmc of SDS. This was observed as an increase in ellipsometric adsorbed amount (Figure 4.6 b), whereas there was a small and large decrease in QCM-D sensed mass and energy

dissipation (Figure 4.6 d), respectively. The collapsed state persisted until the reswelling began at approximately 0.6 cmc SDS. This is in line with the SDS concentration range at which chitosan on highly charged mica is collapsed in a 30 mM $NaNO_3$ solution.[105] Addition of SDS at 1 cmc initiated desorption of chitosan-SDS complexes and major desorption was observed upon rinsing. In 0.1 mM $NaNO_3$ (Figures 4.6 a and 4.6 c), SDS interacts with chitosan already at 0.02 cmc SDS and there is a continuous increase in adsorbed amount, sensed mass, and energy dissipation prior to the observation of desorption of chitosan-SDS complexes at and above 0.6 cmc SDS.

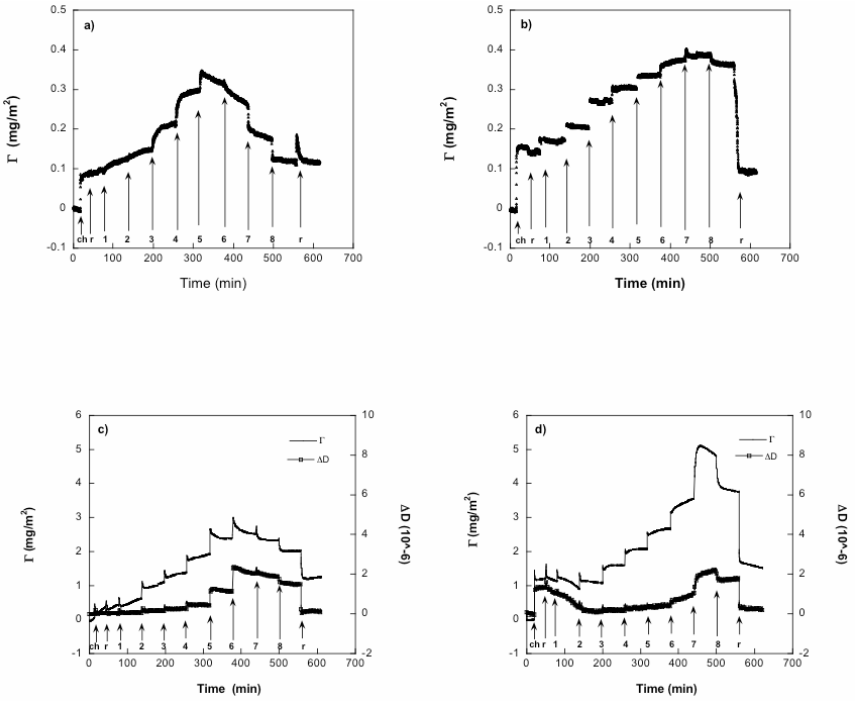

Figure 4.6. *Stepwise adsorption of SDS on a pre-adsorbed chitosan layer. Figures a) and b) show the adsorbed amount from ellipsometry measurements and figures c) and d) the sensed mass (upper curve) and the dissipation (lower curve) obtained from QCM-D measurements at 0.1 mM (a and c) and 30 mM (b and d) of $NaNO_3$. Arrows with the abbreviation* ***ch*** *show addition of chitosan onto a silica substrate and the letters* ***r*** *show rinsing with the background electrolyte solution. The fraction of cmc of SDS is then continuously increased from 0.02 cmc to 1.0 cmc. Arrows number* ***1-8*** *show addition of SDS in the following fractions of cmc:* ***1****)0.02,* ***2****)0.05,* ***3****)0.1,* ***4****)0.2,* ***5****)0.4,* ***6****)0.6,* ***7****)0.8,* ***8****)1.0. All solutions were adjusted to pH 4.0.*

The saturation binding of SDS to chitosan before desorption was calculated from the assumption that no desorption occurs before the total adsorbed amount decreases. Further, the mixed layers are assumed to consist only of chitosan and hence the number of SDS to chitosan is probably a lower estimate of the true value, since the adsorbed amount is proportional to 1/(dn/dc) in Eq. (3.9) and dn/dc is higher for pure chitosan than for SDS. The approach results in a minimum saturation binding of 1.5±0.05 SDS/chitosan in 0.1 mM $NaNO_3$ and 1.01±0.05 SDS/chitosan in 30 mM $NaNO_3$. By considering that this is a lower estimate, it is likely that charge reversal of complexes occurs prior to desorption. The phenomena of charge reversal by adsorption of a cationic polyelectrolyte to negatively charged substrates has been observed and reported several times in the past.[103,26,25] In line with this study, Penfold et *al* showed that adsorption of a cationic polymer reversed the surface charge of silica from negative to positive, to which SDS associated strongly, whereas SDS had no affinity for silica.[97] This recharging process is believed to be the basis for the multilayer build-up of polyelectrolytes with the layer-by-layer method,[22] which is discussed in more detail in the following sections and in papers II, IV, V, and VI.

4.5 Sequential adsorption of biopolymers

4.5.1 Sequential adsorption of BSM and chitosan

In section 4.3, it was shown that chitosan could be sequentially adsorbed onto a pre-adsorbed BSM layer on silica. It was further noticed in paper II, that a multilayer film can be formed by alternating the adsorption of BSM and chitosan, in the sense that there is a linear increase in adsorbed amount with the number of BSM and chitosan deposition cycles (Figure 4.7).[107] However, starting from the 6^{th} layer, overshoots are observed during adsorption of chitosan. That is, the adsorbed amount initially increases upon addition of chitosan, but this is followed by a decrease with time as the layer is exposed to the chitosan solution. This is probably due to re-dissolution of soluble BSM-chitosan complexes into the bulk. An irregular film growth has also been reported during sequential adsorption of chitosan and BSM on hydrophobized silica surfaces.[108] In line with our findings, the adsorption of chitosan induced re-dissolution of BSM-chitosan complexes. In that study, it was also shown that an increased concentration of chitosan in the deposition solution caused an increased film disruption.

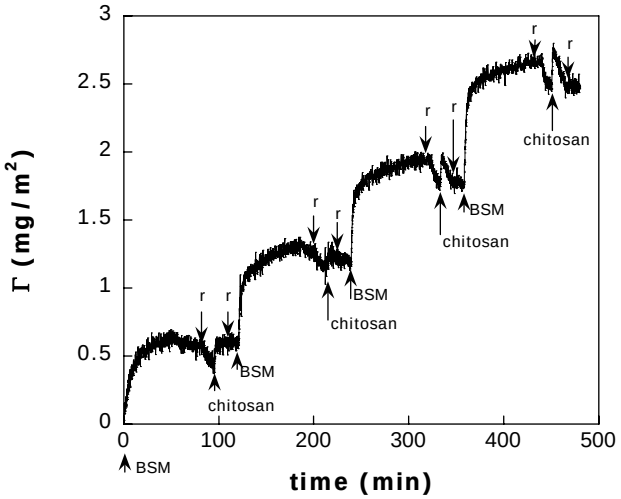

Figure 4.7. *The layer build-up from sequential adsorption of BSM and chitosan on silica surfaces is shown as a function of time. The concentrations of BSM and chitosan were 25 ppm and 20 ppm, respectively. Arrows in the figure mark the additions and the abbreviation, r, indicates rinsing with the 30 mM NaCl background electrolyte solution.*

4.5.2 Sequential adsorption of lysozyme and β-casein

The aim in paper IV was to investigate the possibility of forming a multilayer film containing only proteins. The proteins used were the globular protein lysozyme and the flexible protein β-casein. These measurements were carried out by alternate adsorption of lysozyme and β-casein to a silica substrate at pH 8.5, a pH which ensures that the proteins are oppositely net charged (lysozyme^{+}/β-casein^{-}). The solution deposition ionic strength was varied in the interval 10-150 mM by supplementing a TRIS buffer solution by NaCl. By varying the ionic strength and thereby controlling the electrostatic interactions between the proteins and the substrate, the layer build-up showed a different evolution in adsorbed amount and sensed mass (Figures 4.8 and 4.10).

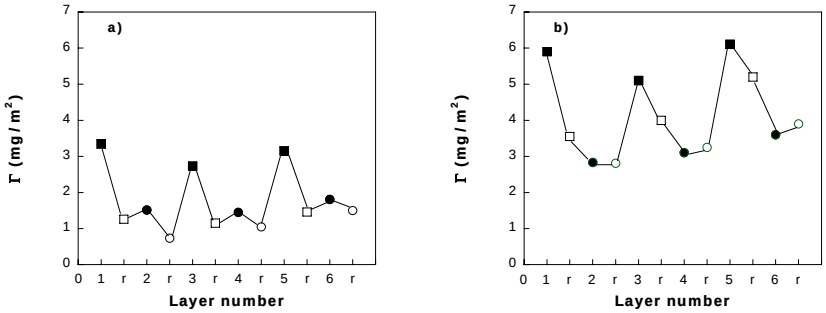

Figure 4.8. *Sequential adsorption of lysozyme and β-casein on a silica substrate, in a TRIS-NaCl buffer at 150 mM (a) and a TRIS buffer at 10 mM (b). The ellipsometry adsorbed amount is shown as a function of the number of adsorption steps where odd and even numbers shows lysozyme (■) and β-casein (●) adsorption, respectively. The abbreviation, r, and open symbols represent the adsorbed amount after rinsing with the protein free buffer solution.*

Figure 4.8 shows the ellipsometric adsorbed amount as a function of the number of adsorption steps during sequential adsorption of lysozyme and β-casein in 150 mM (Figure 4.8 a) and 10 mM (Figure 4.8 b). The build-up is irregular with an adsorption-desorption pattern and only a small increase in adsorbed amount after each deposition cycle. The major difference is that at an ionic strength of 150 mM, each addition of β-casein causes an increase in the adsorbed amount, whereas the total amount decreases at an ionic strength of 10 mM. The increase in adsorbed amount upon addition of β-casein in 150 mM buffer is due to adsorption onto the lysozyme layer, since β-casein has no affinity for silica at this condition (Figure 4.9). However, by rinsing with the protein free buffer solution, most of the increase in adsorbed amount is diminished to approximately the same value as the first lysozyme layer after rinsing. This shows that lysozyme, due to its net positive charge, has a high affinity for the silica surface. At lower ionic strength both lysozyme and β-casein show affinity for silica (Figure 4.8 and 4.9). Hence, it is difficult to judge whether the decrease in total adsorbed amount at low ionic strength is due to adsorption of β-casein on top of lysozyme or displacement of lysozyme by β-casein. However, by comparing the adsorbed amount of β-casein on silica (Figure 4.9) it can be seen that even if the total adsorbed amount decreases, it is still twice as large compared to that of pure β-casein on silica. Therefore, it can be

concluded that the layer after lysozyme and β-casein deposition most likely contains a mixture of the two proteins.

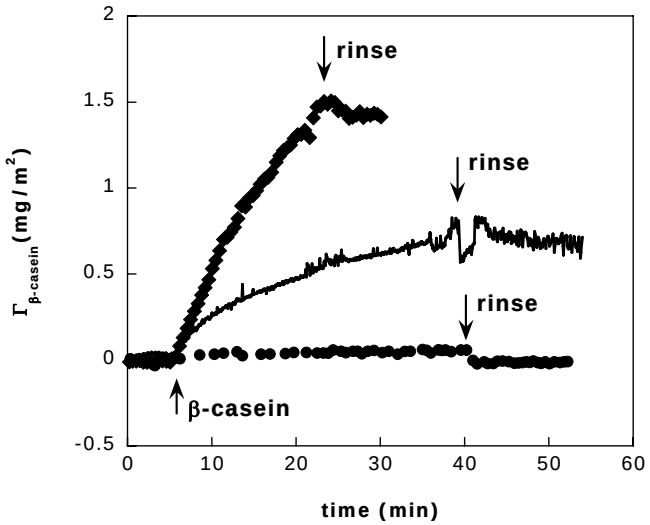

Figure 4.9. *Adsorption kinetics of β-casein (2 mg/ml) at a silica substrate in a TRIS-NaCl buffer of ionic strength 150 (circles), 50 (line) and 10 (diamonds) mM obtained from ellipsometry measurements.*

The QCM-D sensed mass and layer energy dissipation due to sequential adsorption of lysozyme and β-casein at 150 mM, 50 mM, and 10 mM are depicted in Figure 4.10. In line with the results obtained with the ellipsometry technique, there is an increase in sensed mass upon addition of β-casein to a pre-adsorbed lysozyme layer at 150 mM, and a decrease at 10 mM. The adsorption at intermediate ionic strength is qualitatively similar to the results at 150 mM. Changes in energy dissipation are almost the same independent of ionic strength, suggesting that the layer structure depends more on the polyelectrolyte adsorbed in the outermost layer than on solution ionic strength. The low dissipation values of layers having lysozyme adsorbed in the outermost layer compared to the relatively high values obtained for β-casein outer layers before rinse show that lysozyme adsorption favours a more compact layer structure than β-casein, consistent with the fact that lysozyme is globular, whereas β-casein has a random coil structure in solution.

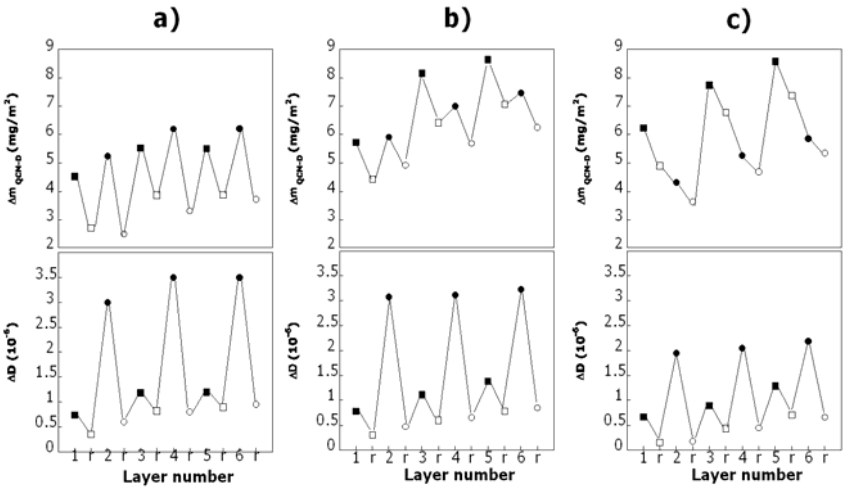

Figure 4.10. *Sequential adsorption of lysozyme and β-casein on a silica substrate, in a TRIS-NaCl buffer at 150mM (a), a TRIS-NaCl buffer at 50 mM (b) and a TRIS buffer at 10 mM. The QCM-D sensed mass and energy dissipation are shown as a function of the number of adsorption steps where odd and even numbers show lysozyme (■) and β-casein (●) adsorption, respectively. The abbreviation, r, and open symbols represent the result after rinsing with the protein free buffer solution.*

The irregular film growth and the low amount of protein adsorbed in each deposition, which is far less than monolayer coverage, suggests a markedly different layer structure compared to those usually reported for multilayers of polyelectrolytes. However, it is important to note that the total adsorbed amount (after rinse) is higher for mixed lysozyme-β-casein layers compared to layers of only lysozyme or β-casein. The protein films probably contain both proteins, but the structure is more an interpenetrated composite rather than a classic multilayer. The difficulty that is encountered with the film formation can be explained by the fact that proteins are not as flexible as linear polyelectrolytes, and the charge distribution in proteins is complex and zwitterionic. The importance of charge has been discussed also in previous reports on the concept of multilayer build-up using proteins.[9,37] The sequential adsorption of two oppositely charged globular proteins was unsuccessful, which was explained by the charge not being overcompensated after each protein deposition.[37] In a recent study where subsequent additions of three different cationic proteins; lysozyme, lactoperoxidase or lactoferrin were carried out to a surface pre-coated with

the anionic mucin (MUC5B) protein showed that the protein pair having similar magnitude of charge formed the most regular build-up.[9] This was the sequential adsorption of mucin (MUC5B) and lactoperoxidase, where adsorption resembled an adsorption-desorption pattern but the adsorbed amount increased with the bilayer number.

4.5.3 Sequential adsorption of chitosan and heparin

The encouraging results of the layer-by-layer assembly using a glycoprotein and a polysaccharide motivated me to make use of two natural polysaccharides for multilayer formation. In papers V and VI, the aim was to explore the structure of a chitosan-heparin film sequentially adsorbed from various solution deposition conditions on silica surfaces. It has previously been shown that a multilayer film of the two polysaccharides has the ability to reduce bacterial adhesion on medical implants where the antimicrobial efficiency depended on the solution conditions used during build-up.[4] The number of bacteria that adhered to the surface was found to decrease with decreasing pH of the polymer assembly solution in the pH range 2.9-6.0 with no added salt. However, the film adsorbed at pH 3.8 was most efficient in killing bacteria that did adhere. The combination of these two polysaccharides in multilayer formations is therefore very interesting for different biomedical applications. For the purpose of understanding the layer structure dependence on pH (pH 4.2 and pH 5.8 were used) of chitosan and heparin layers, we studied the multilayers formed with several techniques: DPI, QCM-D, TIRF, and FRET. The chitosan monomer (saccharide) is approximately 90 % (pH 4.2) and 50 % (pH 5.8) charged due to the primary amine group and a 90 % degree of deacetylation. Heparin in on the other hand fully charged at both pH-values with up to four charges per monomer (disaccharide). Further, the solution ionic strength was either 30 or 150 mM NaCl that provides an additional change in the layer structure due to variations in electrostatic interactions.

The adsorbed amount and layer thickness of the chitosan-heparin films adsorbed from various deposition conditions are shown as a function of layer number in figure 4.11. Contrary to the multilayers formed using proteins, (section 4.5.1 and 4.5.2) the sequential adsorption of these two polysaccharides results in an increased adsorbed amount after each polymer deposition. In line with previous findings, the thickness and adsorbed amount increased when the deposition ionic strength and pH were increased.[109,110,38] Both chitosan and heparin have a relatively high intrinsic stiffness[72,111,88,112] and an increased ionic strength will decrease the electrostatic repulsion between the segment charges, making them less stiff. Thus, the increased adsorption results from the screening enhanced coil

structure. A coiled-like structure of chitosan can also be achieved by increasing the solution pH, since this also reduces the intramolecular repulsion. Even though, the change in solution pH (from 4.2 to 5.8) probably has a minor effect on the heparin structure in solution, it will have an effect on the total film conformation. Previously, Shiratori and Rubner have shown, for weak polyelectrolytes, that if one layer adsorbs in a coil-like conformation, subsequent layers also adopt similar conformations independent of their charge in solution.[109]

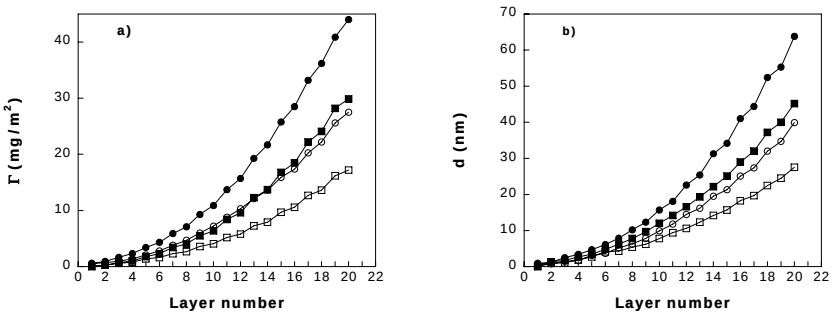

Figure 4.11. *The adsorbed amount (a) and film thickness (b) of the film formed after sequential adsorption of chitosan and heparin to a silica substrate are shown as a function of layer number. All values are reported after rinsing with the electrolyte background solution. In the Figure odd and even numbers represent chitosan and heparin outer layers, respectively. Filled symbols show build-up in solution in 150 mM NaCl at pH 5.8 (circles) or pH 4.2 (squares). Open symbols show the adsorption from a 30 mM NaCl solution at pH 5.8 (circles) or pH 4.2 (squares). Measurements were carried out with the DPI technique.*

4.5.4 Structure of the chitosan-heparin film

Measurements using the QCM-D technique was also carried out on the multilayer build-up, where the sensed mass and thickness were calculated from the Voight equations, Eq. (3.3-3.5) and for comparison also from the Sauerbrey equation, Eq. (3.1). Figure 4.12a shows the evolution in thickness for the chitosan-heparin build-up in solution at pH 4.2 and 30 mM NaCl. Independent of the equation used, there was an adsorption-desorption pattern observed in term of total layer thickness for HEP and CH adsorption, respectively. The decrease in thickness to a value that is lower than that prior to addition in Figure 4.12 is not caused by desorption/redissolution of complexes, as shown for the build-up of

lysozyme and β-casein in Figure 4.10, since the "dry" DPI thickness increases continuously (Figure 4.11). The irregular growth is instead caused by structural changes such as compaction/swelling of the film. By combining the results from the QCM and DPI techniques, we estimated the relative solvent content in these layers according to Eq. (3.6). After comparing the results in Figure 4.12 and 4.13 for the chitosan-heparin layer deposition at pH 4.2 and 30 mM NaCl, we suggested that the decrease in thickness upon CH adsorption was due to water being released from the multilayer film, while again water diffuses into the film upon adsorption of the next HEP layer causing an increased film thickness.

The difference between Voight thickness (d_f) and Sauerbrey thickness (d_{fs}), in Figure 4.12a, is as expected larger for layers with high-energy dissipation (Figure 4.12b). Even though d_f is on average 25 ± 15 % higher than d_{fs} depending on the film energy dissipation (ΔD), the thickness evolutions are very similar. However, since a plot of Sauerbrey sensed mass as a function of the frequency squared for these layers was non-linear and resembled the schematic shown in Figure 3.3, we draw the conclusion that Voight is a better model than Sauerbrey for this system.

The large difference in energy dissipation between overtones indicated that the film has an inhomogeneous structure (Figure 4.12b). In all other QCM-D measurements carried out in this work and to my knowledge also reported in the literature, ΔD_3 is larger than ΔD_5 for an adsorbed film. Therefore, the unexpected behaviour of the chitosan-heparin film prepared at this particular solution condition (pH 4.2 and 30 mM NaCl) showing $\Delta D_7 > \Delta D_5 > \Delta D_3$ (Figure 4.12b) was further analyzed. A more extensive evaluation of the parameters obtained from the Voight model (thickness, shear modulus and viscosity of the film) showed that the change in energy dissipation does not always provide the right viscoeleastic properties (rigid/viscoeleastic) of the film. Instead, the layer viscoelasticity can be determined from the relation between film viscosity and shear as described in paper V.

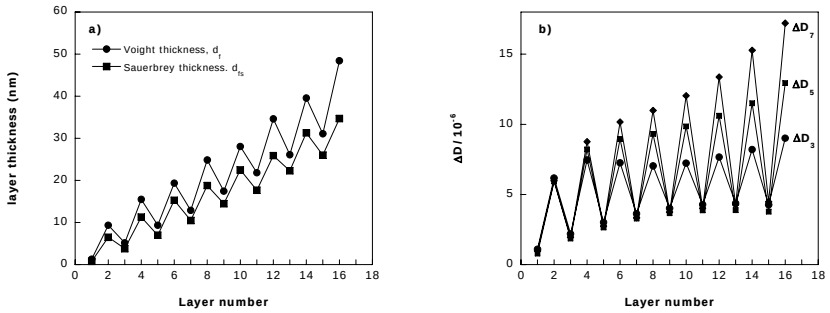

Figure 4.12. *The QCM-D layer thickness of a chitosan-heparin film calculated from the Voight model (circles) or from the Sauerbrey equation (squares) in a). The energy dissipation for the 3rd, 5th and 7th are shown in figure b). Measurements were carried out from a solution of solution ionic strength 30 mM NaCl at pH 4.2. Odd and even number represents CH and HEP outer layers, respectively.*

Figure 4.13 shows that the relative solvent content decreases with the number of deposited layers for all films, independent of the solution deposition conditions. A decreased relative solvent content in the film during build-up has been observed previously for films of the natural polypeptides, PLL/PGA[113]. Furthermore, the difference due to whether chitosan or heparin is adsorbed in the outermost layer becomes less pronounced. However, even after the formation of 12 chitosan and heparin layers, the film is highly hydrated, in the range 60-80 wt-% depending on the deposition conditions. This agrees with the high swelling capacity previously suggested for other polysaccharide based multilayer films that were further found to inhibit cell attachments.[5,6,7] Soft highly hydrated films therefore show favourable properties for avoiding cellular adhesion on for example biomedical implants.

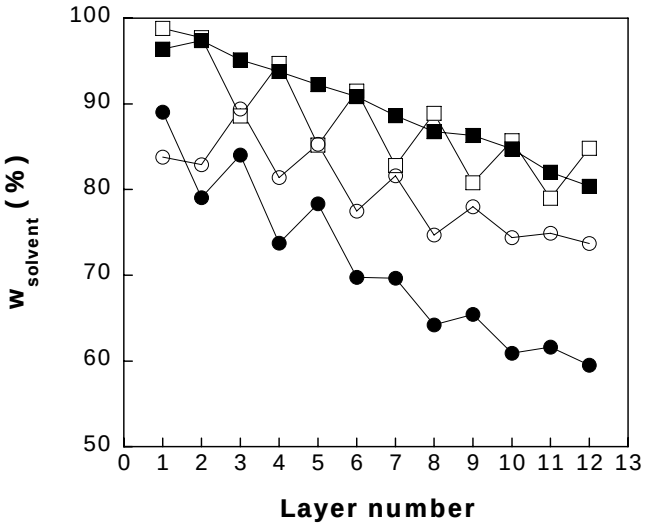

Figure 4.13. *The relative solvent content, $w_{solvent}$, in the film formed during sequential adsorption of chitosan and heparin to a silica substrate are shown as a function of layer number. All values are reported after rinsing with the electrolyte background solution. In the Figure odd and even numbers represent chitosan and heparin outer layers, respectively. Filled symbols show build-up in solution in 150 mM NaCl at pH 5.8 (circles) or pH 4.2 (squares). Open symbols show the adsorption from a 30 mM NaCl solution at pH 5.8 (circles) or pH 4.2 (squares).*

The structure and dynamics of the film was further evaluated by using two fluorescence techniques: total internal reflection fluorescence, TIRF, and fluorescence resonance energy transfer, FRET. Qualitative information about how the film relaxes to accommodate additional layers was obtained with TIRF using the pH-sensitive FITC (fluorescein-5-isothiocyanate) dye embedded within the multilayer film. It is well known that the FITC molecule changes between its prototropic forms depending on the solution pH and on the local electrostatic potential in its close proximity.[114,115] A low solution pH and closeness to a negatively charged substrate or polyelectrolyte will favour protonation, which lowers the fluorescence emission intensity.[114,115]

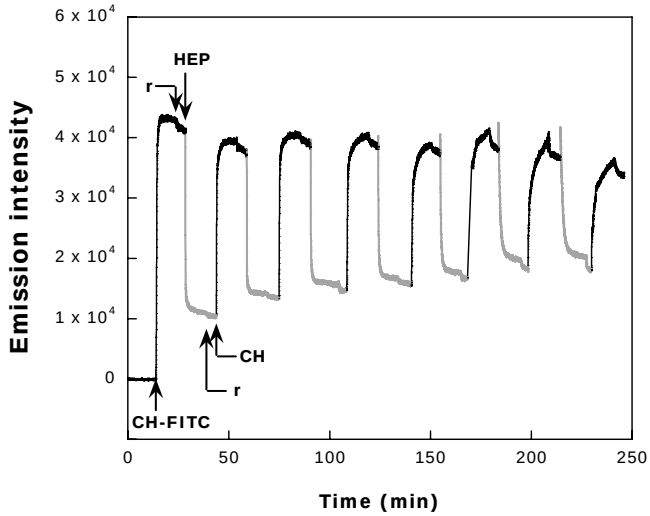

Figure 4.14. *The change in emission intensity due to sequential adsorption of chitosan (CH) and heparin (HEP) to a CH-FITC layer from a 150 mM NaCl solution at pH 5.8. A precursor bilayer of CH/HEP, was pre-adsorbed onto the quartz substrate before the CH-FITC solution was added. After rinsing, indicated by r, the first injection of HEP is made. Subsequent additions of unlabelled CH (black line) and HEP (grey line) produced an increase or decrease in the fluorescence intensity, respectively.*

Figure 4.14 shows that the FITC dye embedded in the chitosan and heparin film is sensitive toward the charge of the polysaccharide that was added last even after 14 sequential adsorption steps of unlabelled chitosan and heparin. Note that changes in emission intensity occur even though neither chitosan nor heparin was labelled in the layers adsorbed on top of the layer containing chitosan-FITC molecules. Variation in ionization state for a weak polyelectrolyte embedded in a multilayer polyelectrolyte film has been observed previously by Fourier transform infrared spectroscopy.[116] The ionization of the weak polyelectrolyte oscillated with the net charge of the outermost layer, changing in the direction that would maintain electroneutrality of the multilayer. We expect that the same thing happen to the carboxyl groups on the FITC molecule. Hence, addition of the negatively charged heparin to the film moves the overall electrostatic potential in a more negative direction, favouring protonation of the fluorescein dye, resulting in a decreased fluorescence emission. Further, the

difference between the intensity maxima and minima decreased slightly after each chitosan-heparin deposition cycle. Similar findings were made in a previous study, showing variations in the emission intensity for multilayer films of two flexible synthetic polyelectrolytes, poly(allylamine hydrochloride) (PAH) and poly(styrenesulfonate) (PSS), containing a buried PAH-FITC layer.[117] However, after deposition of 7 layers of PSS and PAH on top of the PAH-FITC layer, these changes were evened out and for the remaining film formation there were no further intensity changes.[117] This observation was attributed to a gradual densification of the film, whereby the FITC molecules lost their sensitivity to changes in the outermost layer. In contrast, for the chitosan-heparin build-up not even 14 layers of heparin and chitosan were sufficient to reach a constant emission intensity value. We believe that this finding reflects the different internal structure of multilayers prepared from strong synthetic polyelectrolytes displaying a linear growth, compared to the highly hydrated film formed by chitosan and heparin showing an exponential-like growth.

4.5.5 The out-of-plane diffusion of chitosan in multilayer films

The main aim of paper VI was to determine whether the observed exponential-like growth in thickness and adsorbed amount in Figure 4.11 could be attributed to out-of-plane (vertical) diffusion of chitosan molecules within the chitosan-heparin film. It is in fact likely that chitosan is the diffusing species since most of the reported exponential growing films contain either chitosan or poly(L-lysine) (PLL) and confocal laser scanning microscopy (CLSM) has shown that both polymers diffuse in the film.[6,41,42] An interesting observation when comparing these reports is that when hyaluronan is the polyanion, only the polycation (chitosan or PLL) diffuses, whereas both poly(L-lysine) and poly(glutamic acid) diffuse through the entire poly(L-lysine)/ poly(glutamic acid) film.

One problem is that CLSM is restricted to rather thick films[41], whereas the thickness of a 20 chitosan and heparin layer film is less than 70 nm (Figure 4.11). An alternative approach to CLSM for thin films is to study the out-of-plane polyelectrolyte diffusion using the fluorescence resonance energy transfer (FRET)[59, 118] technique. With a characteristic length scale of several nanometers set by the Förster radius (in this study 7 nm), FRET makes it possible to monitor polymer motion on much finer length scales and in much thinner films. In FRET measurements chitosan molecules were labelled by either a donor dye or an acceptor dye. Donor-acceptor energy transfer is extremely sensitive to the distance between the fluorophores and therefore serves as a reporter of changes in proximity of labelled polymers as they diffuse. Both dyes (succinimidyl esters in the Alexa family of

commercially available dyes) were insensitive to local changes in pH. By varying the initial distance, i.e., the number of intermediate layers, between the donor- and acceptor-labelled chitosan molecules in the film, the diffusion path was varied.

Figure 4.15 shows two independent FRET measurements of the chitosan and heparin multilayer build-up in solution at 150 mM NaCl and pH 5.8. This was the deposition condition where the exponential-like growth was most pronounced (Figure 4.11). The chitosan-donor dye molecules are adsorbed in the 5th layer from the substrate and the chitosan-acceptor dye molecules were adsorbed in the 7th or 19th layer according to the schematic. The increased thickness of the intermediate film (from 1.8 nm to 49 nm) should theoretically result in a large decrease in the energy transfer, *E*, according to Eq. (3.11*)*. The Figure demonstrates that chitosan molecules are mobile in the layer after deposition. This is due to a significant and instant energy transfer, *E*, upon addition of chitosan-acceptor dye when the separation is 13 intermediate layers of heparin and chitosan between the initial chitosan-donor placement and the chitosan-acceptor deposition. If the dyes were separated by a distance of 49 nm (Figure 4.11), *E* would have been only 7.5×10^{-4}% according to Eq. (3.11), whereas *E* reaches 25% in Figure 4.15.

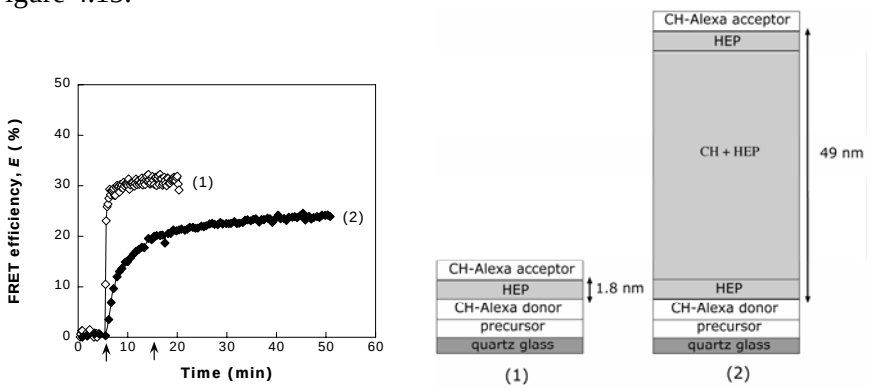

Figure 4.15. *The efficiency of energy transfer, E, between the CH-Alexa 488 and CH-Alexa 555 dye molecules adsorbed in/on a CH-HEP multilayer film prepared in a solution of 150 mM NaCl at pH 5.8. Symbols represent donor and acceptor initially separated by one HEP layer (open diamonds) or 13 CH/HEP bilayers (filled diamonds). These two situations are illustrated by a schematic in the Figure. CH-Alexa 488 was present in layer 5. Arrows mark the addition of CH-Alexa 555 (acceptor dye) and the beginning of a rinse with background electrolyte solution.*

We further evaluated if the chitosan diffusion depends on the polymer deposition solution conditions, hence, on the film structure. FRET measurements were therefore carried out on the chitosan and heparin build-up formed under different solution deposition conditions in Figure 4.16. In all measurements the chitosan-donor dye molecules and the chitosan-acceptor dye molecules were placed in layers separated by 13 heparin and chitosan intermediate layers. However, it is important to note that the thickness of this intermediate film is different depending on deposition conditions (see Figure 4.11 or table-inset in Figure 4.16). The FRET efficiency increases most rapidly in low ionic strength and low solution pH deposition conditions. The key effect of the solution deposition conditions is that the layers are thinner and denser in the low ionic strength, low pH condition. The greater density could be expected to hinder polymer diffusion due to a stronger complexation between chitosan and heparin at these deposition conditions. However, it appears that the thickness of the intermediate polymer film initially separating the two dyes is more important than the actual compaction of the layers, and that the rate of diffusion is in fact not significantly altered as more thoroughly explained in paper VI.

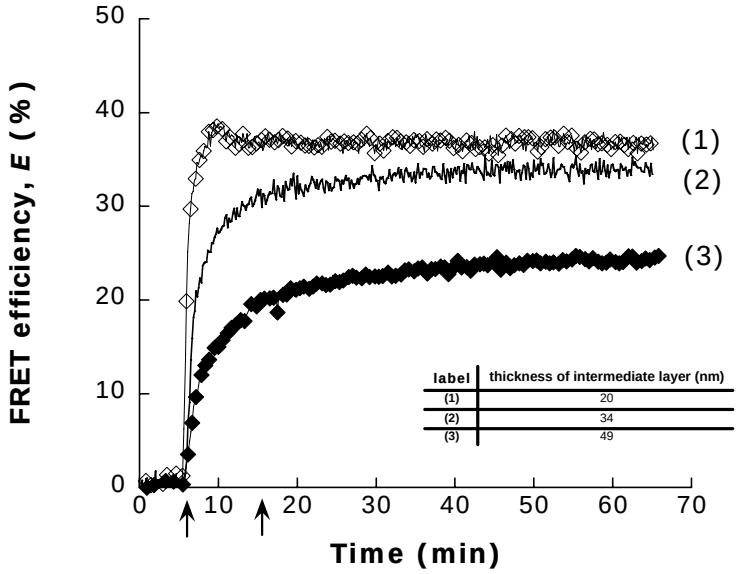

Figure 4.16. *The efficiency of energy transfer, E, between the CH-Alexa 488 and CH-Alexa 555 dye molecules adsorbed in/on a CH-HEP multilayer film. The figure shows three independent measurements where 13 layers of CH and HEP, namely (HEP-CH)$_6$-HEP, were adsorbed in between the layers containing the dyes. The thickness of these layers is shown in the table. Film deposition was carried out from a solution at; 150 mM NaCl pH 5.8 (filled diamonds), 30 mM NaCl pH 5.8 (solid line) or 30 mM NaCl pH 4.2 (open diamonds). Arrows mark the addition of CH-Alexa 555 (acceptor dye) and rinsing.*

5 Concluding Remarks and Future Aspects

The major part of this thesis is based on studies of layer-by-layer (LbL) assembled multilayer films and since this work began the progress in this field has been tremendous. The most interesting aspect of multilayer films is the possibility of combining two or more species (usually polyelectrolytes) and thereby obtaining their individual functions in one film. Since the LbL method has the capacity to incorporate almost all types of high molecular weight species with a large variety of functionalities, there are numerous possible applications for the LbL films. It is generally claimed that the LbL method is simple and cheap, since no advanced equipment is required for film build-up. However, I would like to point out that as the name "multilayer" implies it is quite tedious to prepare the films (even though this multistep process can be automated). For that reason, I believe that the greatest industrial potential for multilayer films is in applications of technologically advanced products, which permits a relatively high price.

During the last decade, the main interest in multilayers has moved from a fundamental interest in the complexation between strong synthetic polyelectrolytes towards film formation using natural polyelectrolytes, such as polysaccharides and polypeptides. Due to their biocompatibility, these films constitute a rapidly growing field. In this thesis work we assembled LbL films containing the natural polysaccharides chitosan and heparin and studied how the physico-chemical properties (such as pH and ionic strength) of the solution affected the growth, structure, and dynamics of the formed multilayer film. In line with what has previously been reported for other natural polymers, the film growth of chitosan and heparin showed an exponential-like increase in thickness and adsorbed amount with the number of deposited layers. One explanation for this behavior has been the interlayer diffusion of at least one of the two polymers in the film during build-up, which has been confirmed with the CLSM technique. However, the chitosan-heparin film (with 20 alternateing layers) was too thin to measure possible polymer interlayer diffusion with CLSM. We therefore applied a different technique, FRET, to prove the vertical interlayer diffusion of fluorescently labeled chitosan molecules within the film. Our results showed that FRET could be a useful complement to the CLSM technique in order to measure interlayer diffusion of a polyelectrolyte in a multilayer film, especially for thin films in the 10 nm to 100 nm range where CLSM is of limited use.

The name “multilayer” film wrongly implies that the film structure is that of lasagne or a sandwich, with discrete layers. Even the strong synthetic polyelectrolytes form layers that have a “fuzzy” structure with diffuse transitions between interpenetrated layers and a polymer distribution width of approximately 3-5 layers. The chitosan-heparin films, show significant interlayer diffusion, and should perhaps be referred to as a “multi-component” film rather than a “mulilayer” film. However, our finding that a pH sensitive dye adsorbed within the film was sensitive to the charge of the outermost layer shows that the polymer adsorbed last has an influence on the entire film. This is in agreement with different film structures (thickness and dissipation) observed for chitosan and heparin terminated layers with the QCM-D technique.

Chitosan-heparin films have previously been suggested for coatings of medical implants (i.e. cardiovascular devises) where the anti-adhesive properties of heparin were combined with the antibacterial properties of chitosan. In that study it was shown that the film deposited at pH 4 was most efficient for these purposes. In this work, we showed that films constructed at this pH had the highest water content (≈ 80 wt-%), which is consistent with what is commonly known to prevent adhesion of bacteria on surfaces. For future aspects it would be interesting to evaluate the antibacterial properties of the films prepared in this study (with different solution deposition conditions of pH and ionic strength) and to find out whether the number of deposited layers in the multilayer has an effect on the anti-adhesive-antibacterial properties of the film. Previous antibacterial tests on heparin-chitosan films were carried out with chitosan adsorbed in the outermost layer, and for that reason it would be exciting to investigate whether a film that has heparin adsorbed last changes the antibacterial efficiency.

In several of the studies carried out in this thesis, we showed the advantage of using the QCM-D technique, which measures the “wet” mass and the energy dissipation, together with a complementary technique that measures the “dry” mass such as ellipsometry or DPI. This combination provides additional information about the water content and more accurate determinations of the film structure. Information obtained from only QCM-D may provide misleading information as shown for the chitosan–heparin film build-up, which showed a stepwise increase-decrease in mass depending on the polysaccharide that was adsorbed last. This would have been interpreted as a stepwise adsorption-desorption pattern if the DPI data had not shown a continuous increase in “dry” mass. The decrease in QCM-

D was therefore attributed to a layer compaction (due to release of water) instead of desorption. Thus, great care has to be taken when evaluating data obtained with the QCM-D technique.

We further showed the importance of using a correct model to calculate the sensed mass from the measured frequency change when using QCM-D. For the highly hydrated and viscoelastic chitosan and heparin film, the mass calculated from the Sauerbrey equation could be underestimated by as much as 40 % compared to the mass obtained from the Voight model. Another outcome of that study was that an increase in energy dissipation could be observed even though the film became more rigid. This was the case for layers displaying higher energy dissipation at higher overtone numbers, but before we make a general statement on this finding, more investigations are needed.

The adsorption studies of mucin (BSM) indicated that the level of purification (e.g. presence of albumin) affected the adsorption and structure of BSM on negatively charged hydrophilic surfaces. An increased amount of BSA in the BSM deposition solution resulted in the formation of a compact/rigid layer of mucin-BSA complexes compared to the highly extended layer formed after adsorption from solutions of pure BSM. The interplay between mucin and other mucous components is an interesting subject considering the large number of nonmucin material present in the mucous environment. We showed that the desorption of a pre-adsorbed BSM layer induced by SDS could be prevented by a protective coating of chitosan. The adsorption of chitosan on mucin induced structural changes in the adsorbed layer such that the SDS binding sites on mucin became blocked. This offers a possible way to protect mucous layers.

Finally, we demonstraded that alternate deposition of mucin and chitosan resulted in a multilayer-like film, whereas alternate deposition of lysozyme and β-casein resulted in protein complexes at the surface, where the adsorbed amount only increased slightly for each lysozyme-β-casein deposition cycle. It would be interesting to find out if the layer build-up could be improved by, for example, lowering the protein deposition concentration, or if the structure of β-casein (surfactant-like) restrains the multilayer formation.

6 Acknowledgments

I would like to express my gratitude to all people, who in different ways have helped and supported me during this work. There are some that I would like to thank in particular.

First of all, my supervisor: **Eva Blomberg**, for your endless encouragement and for always having your door open for discussions about everything. I would also like to thank you for giving me the opportunity to do research in the US, and to attend several international conferences. You are a fantastic and helpful person, and I really enjoyed working with you.

A special thanks to **Robert Tilton,** for sharing your great knowledge of surface chemistry and for all effort in teaching me the fluorescence techniques. My work at the Carnegie Mellon University was very inspiring and I've learnt a lot from our collaboration.

I would like to express my gratitude to **Per Claesson** for providing valuable scientific input in several of the papers and for finding time in a busy schedule to read, and comment on, this thesis.

I would like to thank **Mark Rutland** for initiating my interest in surface chemistry through excellent teaching during undergraduate lectures. Also for having the yearly BBQ-parties at your home and for all attempts to make Swedes more social. Further, I would like to thank both **Mark Rutland** and **Ulla Elofsson** for all scientific guidance during my diploma thesis work and with the paper.

Thank you **Andra Dedinaite** for taking me on the chitosan-mucin project. It was a good and fruitful collaboration, resulting in my first published article.

I would like to thank **Lubica Macakova** for being such a source of inspiration. I learnt so much from you during our struggle with the chitosan-SDS paper, and during all other scientific discussions. But most of all I would like to thank you for being such a good friend.

I would also like to acknowledge my co-authors **Tomas Sandberg, Karin Caldwell, Tommaso Auletta, Faten Solaga, Esben Thormann and Zsombor Feldötö** for valuable input into the work. I enjoyed working with all of you.

Thanks also to all present and former colleagues in the Surface and Corrosion Science group (and former Surface Chemistry group) for all help you have provided and for all the fun we have. I have really enjoyed all interesting conversations in the lunchroom and all the after work activities. I would like to particularly thank **Joseph Iruthayaraj** for all valuable advises on just about everything, for sharing office with me for several years.

Furthermore, I would like to thank all present and former office roommates for lightening up the everyday work.

I am most grateful for all encouragement and support that I have received from my family and friends during these years. Particularly from my parents, **Lars, Marianne** and **Knut-Christian**, my great siblings **Anna** and **Fredrik** and my grandmother **Gun.** Finally I would like to thank my dear **Magnus** for many things and especially for being a great support during the last stressful months of thesis writing.

The SSF-Colintech program is greatly acknowledged for financial support.

7 References

(1) Shi, L.; Ardehali, R.; Caldwell, K. D.; Valint, P. Colloids And Surfaces B-Biointerfaces 2000, 17, 229-239.
(2) Shi, L. Trends In Glycoscience And Glycotechnology 2000, 12, 229-239.
(3) Sandberg, T.; Carlsson, J.; Ott, M. K. Microscopy Research And Technique 2007, 70, 864-868.
(4) Fu, J. H.; Ji, J.; Yuan, W. Y.; Shen, J. C. Biomaterials 2005, 26, 6684-6692.
(5) Elbert, D. L.; Herbert, C. B.; Hubbell, J. A. Langmuir 1999, 15, 5355-5362.
(6) Richert, L.; Lavalle, P.; Payan, E.; Shu, X. Z.; Prestwich, G. D.; Stoltz, J. F.; Schaaf, P.; Voegel, J. C.; Picart, C. Langmuir 2004, 20, 448-458.
(7) Picart, C. Current Medicinal Chemistry 2008, 15, 685-697.
(8) Devlin, J. J.; Panganiban, L. C.; Devlin, P. E. Science 1990, 249, 404-406.
(9) Lindh, L.; Svendsen, I. E.; Svensson, O.; Cardenas, M.; Arnebrant, T. Journal Of Colloid And Interface Science 2007, 310, 74-82.
(10) Haynes, C. A.; Norde, W. Journal of Colloid and Interface Science 1995, 169, 313-328.
(11) Haynes, C. A.; Norde, W. Colloids and Surfaces B: Biointerfaces 1994, 2, 517-566.
(12) Norde, W., Driving Forces for Protein Adsorption at Solid Surfaces. In Biopolymers at Interfaces, 2nd ed.; Malmsten, M., Ed. Marcel Dekker, Inc.: New York, 2003.
(13) Fleer, G. J.; Cohen Stuart, M. A.; Scheutjens, J. M. H. M.; Cosgrove, T.; Vincent, B., Polymers at Interfaces. Chapman & Hall: London, 1993.
(14) Tabak, L. A.; Levine, M. J.; Mandel, I. D.; Ellison, S. A. J. Oral Pathol. 1982, 11, 1-17.
(15) Peppas, N. A.; Sahlin, J. J. Biomaterials 1996, 17, 1553-1561.
(16) Lindh, L.; Glantz, P. O.; Carlstedt, I.; Wickstrom, C.; Arnebrant, T. Colloids And Surfaces B-Biointerfaces 2002, 25, 139-146.
(17) Dedinaite, A.; Bastardo, L. Langmuir 2002, 18, 9383-9392.
(18) Proust, J. E.; Baszkin, A.; Perez, E.; Boissonnade, M. M. Colloids and Surfaces 1984, 10, 43-52.
(19) Perez, E.; Proust, J. E. Journal of Colloid and Interface Science 1987, 118, 182-191.
(20) Feldoto, Z.; Pettersson, T.; Dedinaite, A. Langmuir 2008, 24, 3348-3357.
(21) Iler, R. K. Journal of Colloid and Interface Science 1966, 21, 569-594.

(22) Decher, G.; Hong, J. D.; Schmitt, J. Thin Solid Films 1992, 210, 831-835.
(23) Decher, G. Science 1997, 277, 1232-1237.
(24) Steitz, R.; Jaeger, W.; v. Klitzing, R. Langmuir 2001, 17, 4471-4474.
(25) Caruso, F. Chem. Eur. J. 2000, 6, 413-419.
(26) Blomberg, E.; Poptoshev, E.; Claesson, P. M.; Caruso, F. Langmuir 2004, 20, 5432-5438.
(27) Picart, C.; Lavalle, P.; Hubert, P.; Cuisinier, F. J. G.; Decher, G.; Schaaf, P.; Voegel, J. C. Langmuir 2001, 17, 7414-7424.
(28) Schoeler, B.; Kumaraswamy, G.; Caruso, F. Macromolecules 2002, 35, 889-897.
(29) v. Klitzing, R. Physical Chemistry Chemical Physics 2006, 8, 5012-5033.
(30) Hammond, P. T. Current Opinion in Colloid & Interface Science 2000, 4, 430-442.
(31) Stockton, W. B.; Rubner, M. F. Macromolecules 1997, 30, 2717-2725.
(32) Kotov, N. A. Nanostructured Materials 1999, 12, 789-796.
(33) Bucur, C. B.; Sui, Z.; Schlenoff, J. B. Journal of American Chemical Society 2006, 128, 13690-13691.
(34) Vazquez, E.; Dewitt, D. M.; Hammond, P. T.; Lynn, D. M. Journal Of The American Chemical Society 2002, 124, 13992-13993.
(35) Caruso, F.; Niikura, K.; Furlong, D. N.; Okahata, Y. Langmuir 1997, 13, 3427-3433.
(36) Caruso, F.; Mohwald, H. Journal Of The American Chemical Society 1999, 121, 6039-6046.
(37) Lvov, Y.; Ariga, K.; Ichinose, I.; Kunitake, T. Journal Of The American Chemical Society 1995, 117, 6117-6123.
(38) Dubas, S. T.; Schlenoff, J. B. Macromolecules 1999, 32, 8153-8160.
(39) Kovacevic, D.; van der Burgh, S.; de Keizer, A.; Stuart, M. A. C. Langmuir 2002, 18, 5607-5612.
(40) Lavalle, P.; Gergely, C.; Cuisinier, F. J. G.; Decher, G.; Schaaf, P.; Voegel, J. C.; Picart, C. Macromolecules 2002, 35, 4458-4465.
(41) Picart, C.; Mutterer, J.; Richert, L.; Luo, Y.; Prestwich, G. D.; Schaaf, P.; Voegel, J. C.; Lavalle, P. Proceedings of the National Academy of Sciences of the United States of America 2002, 99, 12531-12535.
(42) Lavalle, P.; Vivet, V.; Jessel, N.; Decher, G.; Voegel, J. C.; Mesini, P. J.; Schaaf, P. Macromolecules 2004, 37, 1159-1162.
(43) Jomaa, H. W.; Schlenoff, J. B. Macromolecules 2005, 38, 8473-8480.
(44) Peyratout, C. S.; Dähne, L. Angwandte Chemie 2004, 43, 3762-3783.
(45) Hammond, P. T. Advanced Materials 2004, 16, 1271-1293.
(46) Tang, Z. Y.; Wang, Y.; Podsiadio, P.; Kotov, N. A. Advanced Materials 2006, 18, 3203-3224.

(47) Vargas, M.; Pastor, C.; Chiralt, A.; McClements, D. J.; Gonzalez-Martinez, C. Critical Reviews in Food Science and Nutrition 2008, 48, 496-511.
(48) Su, Y. L.; Li, C. Applied Surface Science 2008, 254, 2003-2008.
(49) Rodahl, M.; Hook, F.; Krozer, A.; Brzezinski, P.; Kasemo, B. Review of Scientific Instruments 1995, 66, 3924-3930.
(50) Voinova, M. V.; Rodahl, M.; Jonson, M.; Kasemo, B. Physica Scripta 1999, 59, 391-396.
(51) Iruthayaraj, J.; Olanya, G.; Claesson, P. J. Phys. Chem. C 2008, 112, 15028-15036.
(52) Azzam, R. M. A.; Bashara, N. M., Ellipsometry and Polarised Light. 1 st ed.; North-Holland Publishing Company: Amsterdam, 1977.
(53) Landgren, M.; Jonsson, B. Journal of Physical Chemistry 1993, 97, 1656-1660.
(54) Tiberg, F.; Landgren, M. Langmuir 1993, 9, 927-932.
(55) Cross, G. H.; Reeves, A. A.; Brand, S.; Popplewell, J. F.; Peel, L. L.; Swann, M. J.; Freeman, N. J. Biosensors & Bioelectronics 2003, 19, 383-390.
(56) Cross, G. H.; Reeves, A.; Brand, S.; Swann, M. J.; Peel, L. L.; Freeman, N. J.; Lu, J. R. Journal Of Physics D-Applied Physics 2004, 37, 74-80.
(57) Hlady, V.; Reinecke, D. R.; Andrade, J. D. Journal of Colloid and Interface Science 1986, 111, 555-569.
(58) Lassen, B.; Malmsten, M. Journal Of Colloid And Interface Science 1996, 179, 470-477.
(59) Lakowicz, J. R., Principles of Fluorescence Spectroscopy. Plenum Press: New York, 1983.
(60) Stryer, L. Annual Review of Biochemistry 1978, 47, 819-846.
(61) Israelachvili, J. N. Journal of Colloid and Interface Science 1973, 44, 259-272.
(62) Claesson, P. M.; Ederth, T.; Bergeron, V.; Rutland, M. W. Advances in Colloid and Interface Science 1996, 67, 119-183.
(63) Siegbahn, K. Science 1982, 217, 111.
(64) Rojas, O. J.; Macakova, L.; Blomberg, E.; Emmer, A.; Claesson, P. M. Langmuir 2002, 18, 8085-8095.
(65) Binnig, G.; Quate, C. F.; Gerber, G. Phys. Rev. Lett. 1986, 56, 930-933.
(66) Lunkenheimer, K. Journal of Colloid and Interface Science 1989, 131, 580-583.
(67) Delgado, A. V.; Gonzalez-Caballero, F.; Hunter, R. J.; Koopal, L. K.; Lyklema, J. Journal of Colloid and Interface Science 2007, 309, 194-224.
(68) Sauerbrey, G. Z.Phys. 1959, 155, 206-222.

(69) Johannsmann, D. Macromolecular Chemical Physics 1999, 200, 501-516.
(70) de Feijter, J. A.; Benjamins, J.; Veer, F. A. Biopolymers 1978, 17, 1759-1772.
(71) Cuypers, P. A.; Corsel, J. W.; Janssen, M. P.; Kop, J. M. M.; Hermens, W. T.; Hemker, H. C. Journal of Biological Chemistry 1983, 258, 2426-2431.
(72) Lundin, M.; Macakova, L.; Dedinaite, A.; Claesson, P. Langmuir 2008, 24, 3814-3827.
(73) Macakova, L. PhD thesis, Royal Institute of Technology, Stockholm, 2007.
(74) Parker, J. L.; Christenson, H. K.; Ninham, B. W. Review of Scientific Instruments 1989, 60, 3135-3138.
(75) Rojas, O. J.; Ernstsson, M.; Neuman, R. D.; Claesson, P. M. Langmuir 2002, 18, 1604-1612.
(76) Herder, P. C.; Claesson, P. M.; Herder, C. E. Journal of Colloid and Interface Science 1987, 119, 155-167.
(77) Bastardo, L.; Claesson, P.; Brown, W. Langmuir 2002, 18, 3848-3853.
(78) Sandberg, T.; Mellin, L.; Gelius, U.; Caldwell, K. D. Journal of Colloid and Interface Science 2009, 333, 180-187.
(79) Norde, W.; Favier, J. P. Colloids and Surfaces 1992, 64, 87-93.
(80) He, X. M.; Carter, D. C. Nature 1992, 358, 209-215.
(81) Imoto, T.; Johnson, L. N.; North, A. C. T.; Phillips, D. C.; Rupley, J. A., Vertebrate Lysozymes. In The Enzymes, P.Boyer, Ed. Academic Press: New York, 1972; Vol. 7.
(82) Su, T. J.; Lu, J. R.; Thomas, R. K.; Cui, Z. F.; Penfold, J. Langmuir 1998, 14, 438-445.
(83) Walstra, P.; Jenness, R., Dairy Chemistry and Physics. John Wiley & Sons: 1984.
(84) Dickinson, E.; Krishna, S. 2000, 15, 107.
(85) Bastardo, L. A. PhD thesis, Royal Institute of Technology, Stockholm, 2005.
(86) Kumar, M.; Muzzarelli, R. A. A.; Muzzarelli, C.; Sashiwa, H.; Domb, A. J. Chemical Reviews 2004, 104, 6017-6084.
(87) Janes, K. A.; Calvo, P.; Alonso, M. J. Advanced Drug Delivery Reviews 2001, 47, 83-97.
(88) Pavlov, G.; Finet, S.; Tatarenko, K.; Korneeva, E.; Ebel, C. Eur. Biophys. J. 2003, 32, 437-449.
(89) Lane, D. A.; Björk, I.; Lindahl, U., Heparin and related polysaccharides. Plenum Press: New York, 1992; Vol. 313.
(90) Malmsten, M.; Burns, N.; Veide, A. Journal of Colloid and Interface Science 1998, 204, 104-111.

(91) Eriksson, C.; Blomberg, E.; Claesson, P.; Nygren, H. Colloids and Surfaces B-Biointerfaces 1997, 9, 67-79.
(92) Dove, P. M.; Craven, C. M. Geochimica Et Cosmochimica Acta 2005, 69, 4963-4970.
(93) Samoshina, Y.; Nylander, T.; Shubin, V.; Bauer, R.; Eskilsson, K. Langmuir 2005, 21, 5872-5881.
(94) Bolt, G. H. J. Phys. Chem. 1957, 61, 1166-1169.
(95) Sandberg, T.; Blom, H.; Caldwell, K. D. Journal of Biomedical Material Research Part A 2008.
(96) Feiler, A. A.; Sahlholm, A.; Sandberg, T.; Caldwell, K. D. Journal Of Colloid And Interface Science 2007, 315, 475-481.
(97) Penfold, J.; Tucker, I.; Staples, E.; Thomas, R. K. Langmuir 2004, 20, 7177.
(98) Hahn Berg, I. C.; Lindh, L.; Arnebrant, T. Biofouling 2004, 20, 65-70.
(99) Pettersson, T.; Dedinaite, A. Journal of Colloid and Interface Science 2008, 324, 246.
(100) Cardenas, M.; Valle-Delgado, J. J.; Hamit, J.; Rutland, M. W. Langmuir 2008, 24, 7262-7268.
(101) Raynal, B. D. E.; Hardingham, T. E.; D.J., T.; Sheehan, J. K. Biochemical Journal 2002, 362, 289-296.
(102) Shubin, V.; Linse, P. Macromolecules 1997, 30, 5944-5952.
(103) Claesson, P. M.; Ninham, B. W. Langmuir 1992, 8, 1406-1412.
(104) Macakova, L.; Blomberg, E.; Claesson, P. M. Langmuir 2007, 23, 12436-12444.
(105) Dedinaite, A.; Ernstsson, M. Journal of Physical Chemistry B 2003, 107, 8181-8188.
(106) Rinaudo, M.; Pavlov, G.; Desbrieres, J. Polymer 1999, 40, 7029-7032.
(107) Dedinaite, A.; Lundin, M.; Macakova, L.; Auletta, T. Langmuir 2005, 21, 9502-9509.
(108) Svensson, O.; Lindh, L.; Cardenas, M.; Arnebrant, T. Journal of Colloid and Interface Science 2006, 299, 608-616.
(109) Shiratori, S. S.; Rubner, M. F. Macromolecules 2000, 33, 4213-4219.
(110) Boddohi, S.; Killingsworth, C. E.; Kipper, M. J. Biomacromolecules 2008, 9, 2021-2028.
(111) Schatz, C.; Viton, C.; Delair, T.; Pichot, C.; Domard, A. Biomacromolecules 2003, 4, 641-648.
(112) Khorramian, B. A.; Stivala, S. S. Archives of Biochemistry and Biophysics 1986, 247, 384-392.
(113) Halthur, T. J.; Elofsson, U. M. Langmuir 2004, 20, 1739-1745.
(114) Chen, R. F. Archives of Biochemistry and Biophysics 1969, 133, 263-279.
(115) Robeson, J. L.; Tilton, R. D. Langmuir 1996, 12, 6104-6113.

(116) Xie, A. F.; Granick, S. Macromolecules 2002, 35, 1805-1813.
(117) Vonklitzing, R.; Mohwald, H. Langmuir 1995, 11, 3554-3559.
(118) Förster, T. Ann. Phys. 1948, 2, 55-75.